Available online at www.sciencedirect.com
SCIENCE DIRECT®
Ocean Modelling 12 (2006) 46–79
Ocean Modelling
www.elsevier.com/locate/ocemod

A simple convective model of the global overturning circulation, including effects of entrainment into sinking regions

G.O. Hughes *, R.W. Griffiths

Research School of Earth Sciences, The Australian National University, Canberra ACT 0200, Australia

Received 8 April 2004; received in revised form 11 April 2005; accepted 11 April 2005
Available online 13 June 2005

Abstract

We use a simple conceptual model to examine the roles of vertical mixing and surface buoyancy fluxes in the dynamics of the global overturning circulation that ventilates the deep oceans. In addition to using the Munk [Munk, W.H., 1966. Abyssal recipes. Deep-Sea Research 13, 707–730] advection–diffusion balance in the ocean interior, we close the circulation by including the small high-latitude sinking regions, which are assumed to be turbulent geostrophic gravity currents on gentle topographic slopes. The interior and sinking regions are coupled by turbulent entrainment into the sinking regions and we examine the global influence of this entrainment. An important realization is that the rates of mixing into slope currents, predicted to be very small as a function of along-flow distance, imply rates of entrainment per unit depth of fall that are comparable to the entrainment rate for vertical plumes. The overturning mass flux and ocean density stratification are found as a function of the vertical diffusivity and total heat transport. Given a realistic heat transport and the measured average mixing rate of order 10^{-5} m^2/s, this simple model yields predictions consistent with data for the increase in volume flux with depth in slope currents, the magnitude of the global overturning circulation, and the averaged top-to-bottom density difference. Despite the absence of other mechanisms thought to be important in the thermocline, the model also gives a realistic thermal boundary layer thickness. As a consequence of entrainment into the dense sinking currents, the linking of abyssal densities to surface fluxes and the assumption of a uniform diffusivity, the model convective flow requires much

* Corresponding author. Tel.: +61 2 61259957; fax: +61 2 62572737.
E-mail address: graham.hughes@anu.edu.au (G.O. Hughes).

1463-5003/$ - see front matter
doi:10.1016/j.ocemod.2005.04.001

less energy than the Munk (1966) prediction. The results indicate that the ocean overturning is feasibly a convective one and we suggest there might be no need to search for 'missing' mixing.

Keywords: Thermohaline circulation; Meridional overturning circulation; Vertical mixing; Abyssal mixing; Buoyancy forcing; Surface heat fluxes; Slope currents; Entrainment

1. Introduction

Surface waters of the oceans are subject to net heating at equatorial latitudes (between approximately 20°S and 23°N based on a global annualized average) and to net cooling polewards of these latitudes (Houghton et al., 1996, p. 212). The circulation of surface waters, largely driven by wind stress, carries a net poleward transport of heat to maintain the balance. Downwelling occurs at polar latitudes, in highly localized areas, and carries surface waters to abyssal depths (Stommel, 1962; Rossby, 1965; Munk, 1966; Winton, 1995; Pierce and Rhines, 1996; Marotzke and Scott, 1999). This downwelling occurs primarily as dense bottom currents descending against topographic slopes (Spall and Pickart, 2001) in both the northern and southern hemispheres, but surface waters sink to the greatest depth (in the present day circulation) at sites around Antarctica to form Antarctic Bottom Water (AABW). Surface waters that sink in the North Atlantic to become North Atlantic Deep Water (NADW) are found in the abyssal ocean at levels above the AABW. The global overturning circulation is closed by upwelling of the abyssal waters. Some of this upwelling can take place by advection along isopycnal surfaces that outcrop to the surface in the Southern Ocean from depths of up to 1500 m, as a result of wind stress (Tsujino and Suginohara, 1999; Webb and Suginohara, 2001). However, modelling indicates that much of the upwelling can be represented as broadly distributed over much of the ocean area (Stommel and Arons, 1960; Munk and Wunsch, 1998; Tsujino et al., 2000; Hodnett and McNamara, 2003; Scott and Marotzke, 2003), as this requires the minimum upwelling velocity and gives the maximum overturning strength (Winton, 1995).

In current diffusive theories of the meridional overturning circulation (MOC) the density structure throughout much of the ocean is maintained by a balance between slow upwelling of cold water and downward turbulent mixing of heat, for which the required vertical diffusivity (at least at depths between 1000 m and 3000 m) is of $O(10^{-4})$ m^2/s (Munk, 1966; Munk and Wunsch, 1998; Tsujino et al., 2000). Large amounts of mechanical energy (of order 2×10^{12} W) are required to maintain this large rate of vertical mixing. As only the tides and the surface winds can release such amounts of energy (Munk and Wunsch, 1998), it has been argued (Huang, 1999; Wunsch, 2000; Wunsch and Ferrari, 2004) that thermal buoyancy associated with the meridional heat flux cannot be the dominant driving for the overturning circulation, that the circulation cannot be convection, and that heat stored in the relatively warm equatorial surface waters must be carried passively towards high latitudes by the circulation. There has also been an appeal to an interpretation of Sandström's "theorem" (Sandström, 1908). This is actually a postulate that Sandström drew from his laboratory observations with heating and cooling sources placed at opposite ends of a water tank 1 m long and 25 mm wide. Translating the original wording, the postulate states that heating and cooling can maintain a circulation only when the heating is below the level of the cooling

source. This has been taken to imply that heating and cooling at the same level cannot drive a circulation. These two arguments would leave wind stress as the only force available to drive the mean vertical overturning flow.

However, it has been demonstrated that it is incorrect to apply Sandström's postulate to the case of heating and cooling sources at the same geopotential surface. Sandström did not report experiments with this case, but Jeffreys (1925) showed that a convective circulation will be maintained. A number of more recent laboratory experiments and numerical solutions, for rotating and non-rotating cases, with heating and cooling at the same level and distributed over surface areas comparable to the dimensions of the basin, have shown strong convective circulation (Rossby, 1965, 1998; Beardsley and Festa, 1972; Hignett et al., 1981; Park and Whitehead, 1999; Paparella and Young, 2002; Mullarney et al., 2004; Wang and Huang, in press). Hence it is clear that available potential energy can be created and work can be done against friction in such a system, without external mechanical energy supply to mixing, contrary to the thermodynamic arguments of Defant (1961) and Huang (1999). Laboratory experiments with heating and cooling at a sloping base (Wang and Huang, in press) again show a persistent circulation (although only through part of the water depth), evidence that the 1 m sea surface height difference of the oceans between the tropics and the polar regions (Huang, 1999) is not a valid argument against convective flow driven by surface fluxes. Physically, differential heating at the surface generates a pressure gradient in the fluid along the surface, which immediately forces flow as soon as the heating is commenced (Mori and Niino, 2002). In the steady state flow, diffusion in the interior will always transport some heat to the bottom (Mullarney et al., 2004). The cooled plume must inevitably evolve to carry water to the same depth, supplying a matching cooling flux and maintaining the steady state. Relevant to the thermodynamic argument, the heating is then distributed throughout the depth of the flow (unlike the suggestion of Huang, 1999, but consistent with measurements of deep stratification). Cooling, on the other hand, is restricted to the depth of the boundary layer feeding the plume (including deep convection) because the circulation maintains a temperature gradient throughout the remainder of the fluid that is favourable only to downward diffusion of heat. The sea surface height difference cannot influence these flow dynamics. Hence the bulk of the heating is then at a greater depth (pressure) than the cooling. Therefore, it is invalid to apply Sandström's postulate to any system, including the oceans, with heating and cooling sources at the same level. Downward turbulent mixing of the heat will further enhance the circulation. Indeed, Sandström (1908) correctly concluded that a convective circulation will penetrate to the maximum depth of mixing. The numerous laboratory experiments prove that this can be the full-depth of a box, consistent with physical intuition, ocean observations and Munk's (1966) abyssal recipe.

The motive force for the overturning flow should not be confused with the supply of energy for vertical mixing. Turbulent mixing allows transfer of heat to and from the boundary and transports heat downward in the interior, thereby maintaining the stratification and the horizontal density differences (buoyancy forces) available to force circulation. It has been concluded from estimates of the magnitude of the energy required, that mixing (driven by winds and tides) controls the circulation (Munk and Wunsch, 1998; Wunsch, 2000; Wunsch and Ferrari, 2004). However, the importance of mixing does not imply that the circulation is not a convective process. Convection always entails a balance between diffusion from boundaries and internal advection. Maintenance of the ocean stratification requires that the water column is continually overturned by taking dense water to the bottom and advecting the water upward in the interior. This vertical

exchange may be forced by buoyancy. Specifically, buoyancy is the dominant force pushing the dense slope currents that carry deep and bottom waters to their depth of spreading (and we assume here that these currents are the primary sinking legs of the convective overturning). In that case we expect that the surface buoyancy fluxes are central to the problem, and that both mixing rate and buoyancy flux govern the rate of overturning. Many GCM studies of the MOC (e.g. Wright and Stocker, 1991; Suginohara and Aoki, 1991; Rahmstorf, 1996; Tsujino et al., 2000; Park and Bryan, 2001; Rahmstorf, 2003) support a convective nature for the overturning, with particular attention to sinking in the North Atlantic and a vertical advection–diffusion balance in the Pacific.

Our purpose in this paper is to use an analytical model to examine a purely convective circulation, in which buoyancy is the motive force for the overturning and in which (as with any other form of convection) buoyancy flux and diffusion act together to govern the flow. The approach taken here is very different from the boundary layer analyses for horizontal convection (forced by fluxes on the same horizontal surface) by Rossby (1965), Killworth and Manins (1980), Hignett et al. (1981) and Whitehead and Pedlosky (2000), and provides further insights into the fundamental dynamics of horizontal convection. Wind forcing can drive some of the meridional heat transport in the upper ocean and it can supply energy to turbulent mixing in the interior, but we will neglect any further roles of wind in forcing the overturning, such as through Ekman pumping. Thus we derive an estimate for the overturning mass flux and ocean density profile that would be produced by buoyancy forcing (i.e. convection), in the presence of interior vertical mixing and entrainment into the sinking regions. The results are compared with the observed MOC, and with previous scaling laws and idealized GCM studies.

A second outstanding question relevant to the MOC is a discrepancy between measured and predicted rates of vertical mixing. Dissipation and tracer measurements in the ocean interior (Gregg, 1989; Ledwell et al., 1993; Kunze and Sanford, 1996; Matear and Wong, 1997) support a much smaller vertical diffusivity (of order $10^{-5}\,\mathrm{m^2/s}$) compared to that required by the Munk and Wunsch approach. Recent data (Rudnick et al., 2003) also suggest that the basin-averaged diffusivity is less than a factor of three above that in the interior, despite the discovery of regions of very intense turbulence associated with topography (Polzin et al., 1997; Lueck and Mudge, 1997; Ledwell et al., 2000). We will consider a range of diffusivities when evaluating the roles of interior mixing and surface buoyancy fluxes.

In order to understand the combined roles of vertical diffusion and surface fluxes we require a new model in which the circulation is closed by linking the interior flow with the surface fluxes and with the localized regions of sinking. The deep sinking mostly takes the form of sill overflows from marginal seas, such as the Weddell Sea and Denmark Strait–Faroe-Bank, and semi-geostrophic dense currents flowing down bottom slopes (Price and Baringer, 1994; Jiang and Garwood, 1996; Swaters, 1998; Killworth, 2001). There may also be a net downward volume flux associated with deep convection in the open ocean in the North Atlantic (see Winton, 1995; Send and Marshall, 1995; Visbeck et al., 1996; Marotzke and Scott, 1999), but even there GCM studies have indicated that boundary sinking is likely to be the most important (Spall and Pickart, 2001). The conclusions in this paper, however, do not depend on the exact form of the sinking. Indeed similar conclusions can be reached by considering a simple vertically-falling plume.

A poor understanding of dense slope currents (e.g. their path, stability, spreading and mixing) makes them an active area of research (Killworth, 2001; Legg et al., in press). The currents are

generally considered to be gravity currents and to be turbulent as a result of bottom shear stress. The turbulence will cause entrainment (or horizontal withdrawal) of surrounding waters from the surrounding ocean density stratification (Speer and Tziperman, 1990). Given that the Antarctic plume(s) reaches the bottom (while the NADW does not), and using the simplification that the AABW tends to fill the global ocean as a single basin, the results of many turbulent plume studies in relatively simple, Boussinesq systems (Baines and Turner, 1969; Killworth and Turner, 1982; Wong and Griffiths, 2001) imply that this plume carries the greatest buoyancy flux and is likely to be dominant in producing the globally-averaged top-to-bottom density difference. The same reasoning indicates that the North Atlantic sinking presently has a smaller buoyancy flux (but not necessarily a smaller volume flux) and that its spreading takes place within the stratification established by the dominant plume. An important aspect for climate research is that this weaker plume is then likely to have the most variable depth of penetration in response to changes in surface forcing. A non-linear equation of state for seawater, regional differences in the properties of ambient waters entrained into each sinking current, and perhaps different topographic slopes and current paths, will complicate the behaviour, but the simple model has great value in providing a framework on which to build.

The role of mixing into overflows and slope currents in the larger-scale overturning circulation has been examined in recent GCM-based studies of the North Atlantic, but the results are not conclusive. For example, Döscher and Redler (1997) indicate a sensitivity of the large-scale circulation to convective mixing, whereas Thorpe et al. (2004) find little sensitivity to the mixing parameterization. In any case, these models use convective parameterizations for flow sinking on a discretely stepped topography and as such do not reliably represent the turbulence and level of mixing in currents having internal density stratification and flowing on gentle slopes. They also do not address the global ocean or the dominant sinking plume (the Weddell Sea Outflow) that feeds the bottom waters.

Hydrographic data for the major slope currents show that there is a large increase in transport with depth (Price and Baringer, 1994; Orsi et al., 1999, 2002), and it would therefore appear that entrainment results in a crucial contribution to the mass flux and properties of deep and bottom waters. These observations suggest the possibility of significant recycling of waters between the interior and the sinking regions at abyssal depths, without requiring all of the mass flux to upwell through the thermocline. Such a picture is a significant departure from the requirement that there be a one-dimensional balance of advection and diffusion in the deep interior, and highlights the importance of developing better conceptual and process models for the circulation, as well as further improving the parameterization of mixing into sill overflows and slope currents in GCMs. The existing understanding of turbulent entraining plumes and the so-called "filling box" process of Baines and Turner (1969) offers some immediate insights into the way in which the dense currents may interact with their surroundings, with a dominant plume building the stable ocean stratification from below. However, this process continually adds density to the bottom, gives only unsteady solutions and does not include interior vertical diffusion.

In this paper we develop a simple dynamical model with which to examine, as a function of the vertical diffusivity, the form of steady overturning circulation that can be supported by buoyancy forcing at the surface. As a first approximation to the global ocean, and in the interests of illustrating the principles, we describe the circulation involving only a single slope plume (representing the southern hemisphere in the present circulation). Other slope plumes will have

comparable fluxes if they are to have global significance. However, the weaker plumes will intrude at shallower depths (e.g. the NADW) and have relatively small effects on the stratification (Killworth and Turner, 1982; Wong and Griffiths, 2001). An important aspect of the solution is that the large-scale circulation and the sinking (slope current) dynamics are fully coupled, via the surface fluxes, i.e. the plume evolution is influenced by the ambient density structure which, in turn, is influenced by the plume. We develop in Section 2 an analytical solution for the circulation (which we refer to as a "recycling box" to emphasize the concept of a steady, diffusive "filling box" with zero net heat flux). This model has aspects in common with an analysis of entraining slope currents from marginal seas by Speer and Tziperman (1990), but we include matching heating and cooling fluxes distributed over the surface of the global ocean. We then apply the model to the oceans, in Section 3, focusing on the model predictions for diffusivities of 10^{-5} m^2/s, as measured in the ocean interior, and 10^{-4} m^2/s, as predicted by the Munk (1966) balance. The solutions confirm that entrainment reduces the interior mixing rate required to sustain a given stratification, and suggest that the larger turbulent diffusivities may not be necessary to maintain the observed overturning circulation. We predict for the measured mixing rates, a convective overturning mass flux and rates of entrainment into the slope current consistent with ocean measurements, as well as a vertical density distribution similar to the globally-averaged density profile in the oceans. Thus the solutions show that the observed circulation is plausibly a convective flow forced by the surface heat fluxes, in the presence of the smaller diffusivity. For a given top-to-bottom average density difference, the external energy input required for mixing is an order-of-magnitude less than that predicted for the diffusivity of Munk and Wunsch (1998). In Section 5 we reconcile our results with the previous larger estimates for the vertical diffusivity in the oceans.

2. A 'recycling box' model for the global overturning circulation

2.1. Approach and assumptions

We now develop a description of the circulation in the simple model of Fig. 1. The model builds on earlier conceptual models of the thermohaline circulation consisting of a few localized downwellings extending to the bottom and a broad, slow upwelling. Vertical mixing in the interior (everywhere outside the sinking plume) is required to maintain a steady density distribution and is characterized by an arbitrary but uniform diffusivity $\overline{\kappa^*}$ that can, in the general case, be molecular or turbulent. For turbulent diffusion we do not specify the energy source, which may include the winds and tides.

Following previous discussions of the dynamics and mixing in ocean bottom currents (Price and Baringer, 1994; Jiang and Garwood, 1996; Killworth, 2001), we assume a buoyancy–bottom drag momentum balance, with the mixing into the slope currents predominantly forced by the mean along-stream shear stress. This assumption allows entrainment rates to be estimated from Taylor's entrainment assumption (Turner, 1986). A large additional input of energy to the current from internal tides and waves impinging on the slope might imply a greater entrainment rate that is not taken into account here. Our assumption is also consistent with the recent convection experiments of Mullarney et al. (2004), which show that at sufficiently

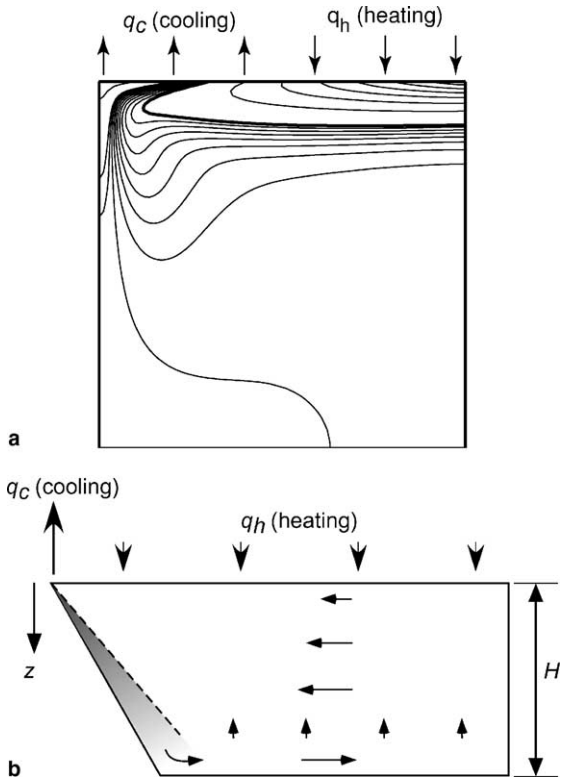

Fig. 1. Convective flows owing to cooling and heating at rates q_c and $q_h = -q_c$, respectively, along the same horizontal boundary. The surface cooling leads to a small region of downwelling from the surface to the bottom, and surface heating allows the flow to reach a steady state: (a) isotherms in a square box obtained from a numerical simulation of horizontal convection driven by an imposed linear temperature gradient along the surface for a Rayleigh number of 10^6 (Mullarney, 2004, cf. Rossby, 1998). Similar solutions are found at much higher Rayleigh number (Mullarney et al., 2004); (b) schematic diagram of a model for the meridional overturning circulation of the oceans. The downwelling is represented as a slope plume in an idealized ocean of depth H and cross-sectional area A. Only the downwelling with greatest buoyancy flux is shown. If the sinking is turbulent, entrainment drives recirculation at depth. For analytical purposes, the cooling is treated as at a point and heating is then over the entire area.

large Rayleigh numbers the (full-depth) downwelling plume against the boundary (and the bottom outflow) can be turbulent in appearance, entraining water from its surroundings even under laboratory conditions. We note that buoyancy-driven turbulent currents would appear to be inconsistent with the Paparella and Young (2002) prediction that horizontal convection is non-turbulent. Their conclusion is based on the result that the basin-averaged dissipation rate vanishes in the inviscid limit (when both molecular viscosity and molecular diffusivity vanish). For now we simply note that the sinking occupies a very small fraction of the basin volume (and say nothing about the role of buoyancy on the basin-averaged mixing) and that entrainment does not require fully-developed turbulence. Our description of sinking regions as slope currents strictly applies only at depths greater than the sill depth from which the plume begins its travel downslope. However, we assume the plume has a point source at the ocean surface

because that is where the vertical volume flux must be zero, and because the surface water (with the maximum density) must sink. Thus we avoid the tasks of describing the specifics of convection and mixing in the marginal sea or on the continental shelf. In any case, wind-driven mechanisms are expected to influence the shape of the density profile in the thermocline. Hence the model is expected to be a crude approximation at shallow depths, perhaps useful only for the density difference. On the other hand, we have found that a similar formulation of the model assuming a region of turbulent vertical sinking to the bottom in the open ocean, in place of the slope current, leads to comparable results. Although the formulation for an overturning flow with a vertical plume is simpler, we report here the case with a slope plume as it has greater oceanographic relevance.

We treat the cooling flux q_c at the surface as entirely focussed into the plume at one end of the basin (Fig. 1b), and distribute the heat input uniformly over the entire surface. The localization of cooling is for analytical convenience only—the exact position of the cooling and the size of the cooling area will not play an important role in determining the pattern of flow or the density stratification, provided there is no net heat input and the resulting distribution of temperature along the surface is monotonic. A two-dimensional formulation of this model (to be reported elsewhere) has been applied to the tank experiments of Mullarney et al. (2004), where one half of the boundary is cooled, and gives excellent agreement. Somewhat similar circulation occurs in the "filling box" flow (Baines and Turner, 1969; Killworth and Turner, 1982; Pierce and Rhines, 1996). However, in these "filling box" studies the density was not constant in time owing to the continual addition of buoyancy from the plume source. Here we require a matching heat input $q_h = -q_c$ distributed over the surface, and we allow for vertical diffusion of heat (density) in the interior. Both the flow and the density profile reach a steady state in which diffusion and advection of density are exactly balanced in the interior. Importantly, we allow the vertical upwelling velocity in the ocean to vary with depth, a consequence of the entrainment of water into the turbulent currents carrying cold waters to the bottom. We derive in this section a set of coupled equations for the slope current and the ocean interior, for which the solution (given the observed heat flux) involves one free parameter—the interior vertical diffusivity.

The isopycnal surfaces in the interior of a convective overturning flow driven by surface fluxes must outcrop to the surface in the area of cooling as the flow approaches the sinking region (Fig. 1a). This outcropping occurs because the poleward surface flow must lose buoyancy to the surface before it can sink at the plume, and the densest water in the system is found at the surface above the plume. With the model idealization of cooling at a point source, this outcropping occurs at the edge of the plume, leaving the isopycnals flat throughout the interior (Fig. 1b). In the laboratory experiments of Rossby (1965) and Mullarney et al. (2004), where the destabilizing heat flux is distributed over a finite area of the surface, isotherms are seen to slope upward (inverting the experiments to the ocean orientation) from the interior to outcrop at the surface across the 'cooled' area and in the vicinity of the plume. In the case of an applied temperature gradient (Rossby, 1965, 1998) the outcropping can form a tight surface front. In these non-rotating experiments, as well as in rotating experiments (Hignett et al., 1981; Park and Whitehead, 1999; Whitehead and Pedlosky, 2000), the outcropping density surfaces are qualitatively similar to those measured in the oceans (e.g. Peixoto and Oort, 1992, p. 195). For example, the neutral density surfaces at depth in the Southern Ocean slope upward at latitudes polewards of 50°S to approach the surface near Antarctica. Likewise, both the tank experiments and the ocean show a reduced vertical density

gradient at shallow depths near the sinking compared with the same depth in the interior. Water is cooled by transport of heat to the surface (by mechanisms including mixed-layer and deep convection, but modelled most simply here in terms of a uniform diffusivity). Returning to the model formulation, the cooling and outcropping are simply compressed into a region at the edge of the plume. Thus the model given here captures the way in which sinking regions entrain surrounding water having abyssal densities at shallow depths.

Planetary rotation is expected to play an important dynamical role in the (near horizontal) flow of turbulent bottom currents on a slope and we include this explicitly in our representation of a geostrophic mean flow in the three-dimensional bottom current. However, as a first approximation, we do not include effects of rotation in the interior (zonally-integrated) flow on the grounds that the isopycnal surfaces are observed to be flat throughout much of the ocean interior (presumably owing to a large difference between the short timescales for horizontal homogenization and the millenial timescale for vertical flow). The flat isopycnals, in turn, imply that the formulation does not require consideration of a horizontal momentum equation in the interior or surface boundary layer. Instead, the use of an imposed (or observed) total heat transport and the consequent horizontal pressure differences at the plume are sufficient to close the problem. Hence the simple geostrophic scaling, previously invoked to explain the dependence of heat and mass fluxes on surface temperature difference and vertical diffusivity in GCM studies of the overturning circulation (Bryan and Cox, 1967; Bryan, 1987; Wright and Stocker, 1991; Park and Bryan, 2001), does not enter explicitly. The use of the observed heat flux as a boundary condition in the present model, however, implicitly involves the wind-driven geostrophic flow, Ekman transport and planetary vorticity dynamics of the surface layer. Hence the models may be consistent with each other. Rather than predict the heat flux as a function of a surface temperature difference, the present approach aims to solve for the vertical overturning flow as a function of the heat flux. We return to this point in Section 4.

In the interests of illustrating a simple means of estimating the ocean overturning and most simply demonstrating the potential role of entrainment, we make several idealizations. We present a formulation with a horizontal basin area independent of depth (but also report the effects of a changing area in Section 4). We also neglect effects due to a non-linear equation of state. A second sinking region, such as the present North Atlantic, is omitted. This can be included, and introduces the ratio of the two buoyancy fluxes as an additional parameter, along with cross-equatorial flow and the question of whether steady states then exist. Space does not allow this extension to be reported here and it is not central to illustrating the effects of entrainment or to estimating, to order-of-magnitude, the overturning owing to any of the major sinking regions. Earlier models incorporating a vertical diffusion–advection balance and entrainment of ambient water into a plume or bottom current (Manins, 1973, 1979; Speer and Tziperman, 1990; MacCready et al., 1999) have used even simpler geometries and dynamics to describe the plume. These models have not been applied to the global ocean. For instance, Manins (1973) analyzed the circulation owing to a vertical line plume in a rectangular box and compared solutions with observations of the density stratification in the Red Sea, with favorable results. However, his formulation allowed the adjustment of three free parameters when fitting the model to the measured density profile. Speer and Tziperman (1990) applied similar ideas to a source of dense water flowing into an ocean basin, using a streamtube model for the slope current, but did not impose a vanishing net surface buoyancy flux to allow the system to be steady.

2.2. The slope plume

We develop the equations describing conservation of volume, momentum and buoyancy for the turbulent slope current illustrated in Fig. 2. Currents on a topographic slope φ are in approximate geostrophic balance and their downslope trajectory is usually at a small angle to the contours of constant depth (Killworth, 2001). We assume that the lateral current width $2R$ is much greater than its height, and that both the mean along-stream velocity $\overline{U}$ and the mean density $\overline{\rho}$ in the current approach ambient values as the normal distance z' from the slope increases. Following Baines and Turner (1969) and Turner (1973) we approximate $\overline{U}$ and the density anomaly $\overline{\rho} - \rho_e$ by a Gaussian form,

$$\overline{U}(s,z') = U_s(s)\exp\left[-\frac{z'^2}{B^2(s)}\right] \tag{1}$$

and

$$\overline{\rho}(s,z') - \rho_e(s) = [\rho_p(s) - \rho_e(s)]\exp\left[-\frac{z'^2}{B^2(s)}\right], \tag{2}$$

where s is the along-stream coordinate and $B/\sqrt{2}$ is the $1-\sigma$ height of the current. For (2) to be valid, we assume B to be much less than the vertical scale over which the density ρ_e in the basin interior varies, and $\rho_e(s)$ is then the density of water in the basin at the depth corresponding to the along-stream position s in the slope current. The volume flux in the slope current increases with distance s owing to entrainment of ambient water.

The entrainment flux is characterized by a ratio E_θ of an entrainment velocity to the streamwise current velocity, where the entrainment velocity is defined by the rate of increase of the current volume flux per unit width (Baines and Turner, 1969; Turner, 1973). Thus the volume flux per unit width in the current increases with s at a rate $E_\theta U_s$, where the entrainment constant is determined

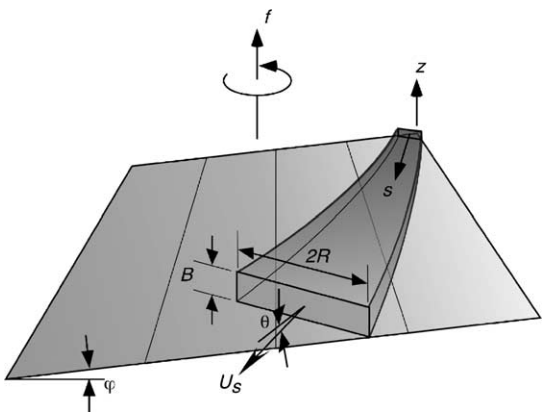

Fig. 2. Schematic diagram of a turbulent bottom current on a topographic slope φ. The angle that the along-current direction makes with its projection onto the horizontal plane is θ. Bottom friction is assumed to maintain turbulence throughout the depth of the current, while larger-scale eddying motions across the width of the current are assumed to be governed by planetary rotation.

by the angle θ that the (along-current) slope makes with the horizontal and the Richardson number of the current (Turner, 1973, p. 179),

$$Ri = \frac{g(\rho_p - \rho_e)B\cos\theta}{\rho_r U_s^2}, \tag{3}$$

where g is the gravitational acceleration and ρ_r is a reference density. For non-rotating downslope flows and θ ($=\varphi$) less than about 5° Ri is of O(0.5) or more (Turner, 1973). The force balance operating in the along-stream direction at small θ and $Ri \gtrsim$ O(1) is between bottom friction and buoyancy (Turner, 1973), and for geostrophic slope currents Killworth (2001) calculates an upper bound on the rate of descent on the slope as

$$\sin\theta \lesssim \frac{1}{400}, \tag{4}$$

where θ is defined to be the angle between the along-current direction $\hat{s}$ and its projection onto the horizontal plane. Eq. (4) is consistent with slope currents in the Weddell Sea, which have an average slope of $\theta \approx 0.1°$ (descending 2500 m along the outflow path of length 1500 km, Price and Baringer, 1994). Under these conditions E_θ is small (Turner, 1973), but not zero (as assumed by Price and Baringer, 1994; MacCready et al., 1999).

Upon integrating (1) over the current cross-section, we obtain the equation describing the volume flux in the slope current,

$$\frac{d}{ds}\left[\frac{\sqrt{\pi}}{2}BRU_s\right] = E_\theta R U_s. \tag{5}$$

Following Killworth (2001) the momentum balance for the current in the $\hat{s}$-direction may be expressed as

$$C_D U_s^2 = \frac{g(\rho_p - \rho_e)}{\rho_r} B\sin\theta, \tag{6}$$

where C_D (≈ 2–3×10^{-3}) is the drag coefficient. Together with (4), Killworth (2001) then finds slope currents to be well represented by a Froude number criterion of the form

$$U_s^2 = c_1 \frac{g(\rho_p - \rho_e)}{\rho_r} B, \tag{7}$$

where c_1 is a constant taking a value approximately equal to one. Following Turner (1973) the equation describing the buoyancy of the current may be written

$$\frac{d}{ds}\left[\frac{BRU_s}{\sqrt{2}}\frac{g(\rho_p - \rho_e)}{\rho_r}\right] = BRU_s\frac{d}{ds}\left[\frac{g(\rho_r - \rho_e)}{\rho_r}\right], \tag{8}$$

using (1) and (2).

Entrainment into bottom slope currents is poorly understood. To find E_θ at small θ we apply a linear interpolation between $E_\theta \approx 10^{-2}$ at $\theta = 5°$ (Turner, 1973) and the theoretical limit $E_\theta \to 0$ at $\theta = 0°$. For $\theta = 0.1°$ we interpolate $E_\theta \sim 2\times10^{-4}$, which is consistent both with that expected (Turner, 1973, p. 182) for slope currents in the Weddell Sea based on their bulk Richardson number ($Ri \sim 3$, calculated using $\rho_p - \rho_e \sim 0.03$ kg/m^3, $\rho_r \sim 1025$ kg/m^3, $B \sim 100$ m, and

$U_s \sim 0.1$ m/s, Price and Baringer, 1994) and with recent data characterizing numerous dense outflows in the oceans (Price et al., 2003).

The above ad hoc estimates for E_θ are consistent with those expected from a scaling analysis. Combining (5) and (8) gives

$$E_\theta = \sqrt{\frac{\pi}{2}} \frac{B}{(\rho_p - \rho_e)} \frac{d}{ds}\left[(\rho_r - \rho_e) - \frac{(\rho_p - \rho_e)}{\sqrt{2}}\right]. \tag{9}$$

Assuming that the top-to-bottom density difference in the basin interior is comparable with the density anomaly in the slope current near the surface, we expect from (9) that

$$E_\theta \sim \sqrt{\pi}\frac{B}{S}, \tag{10}$$

where S is the total along-slope distance travelled by the current. For slope currents in the Weddell Sea, (10) predicts $E_\theta = O(10^{-4})$. Some evidence indicates that the entrainment constant may vary with depth (e.g. near a break in bottom slope, Price and Baringer, 1994).

The along-stream coordinates (s, z') can be transformed to the locally horizontal–vertical coordinate system (x, z). For this purpose we define the entrainment constant

$$E_z = E_\theta / \sin\theta, \tag{11}$$

which is the rate of increase with vertical distance of volume flux per unit width in the current (cf. Eq. (9) with $ds \sin\theta = dz$). It is remarkable that for the small slopes and values of E_θ characterizing outflows in the ocean $E_z \approx 0.1$, which is the same as the entrainment constant for a vertical plume (Baines and Turner, 1969; Turner, 1986). In the absence of a better model we therefore take a constant value $E_z = 0.1$ for slope currents. We expect this might over-estimate the entrainment rates at greater depths, where slopes tend to be smaller and the current has grown thicker. However, the solutions for constant E_z will show that entrainment is small at depths greater than 2500 m, so that the results are insensitive to the value used at those depths.

We express (5), (7) and (8) in terms of the vertical plume velocity W_p, which is the vertical component of the along-stream velocity U_s,

$$\frac{d}{dz}\left[\frac{\sqrt{\pi}}{2} B R W_p\right] = E_z R W_p, \tag{12}$$

$$W_p^2 = c_1 \frac{g(\rho_p - \rho_e)}{\rho_r} B \sin^2\theta, \tag{13}$$

and

$$\frac{d}{dz}\left[\frac{B R W_p}{\sqrt{2}} \frac{g(\rho_p - \rho_e)}{\rho_r}\right] = B R W_p \frac{d}{dz}\left[\frac{g(\rho_p - \rho_e)}{\rho_r}\right]. \tag{14}$$

We require a description for the rate of lateral expansion of the turbulent bottom current along its path. Once the current is in approximate geostrophic balance (Killworth, 2001), instabilities generally develop and effectively increase its width. Although both downslope drainage in the bottom Ekman layer and motion of the ambient water column can play a role in this lateral expansion (e.g. see Sutherland et al., 2004), we neglect these effects and concentrate on the baroclinic instability driven by buoyancy forces associated with the dense current, as observed by Swaters (1991, 1998),

Jiang and Garwood (1996), Etling et al. (2000) and Choboter and Swaters (2000). In these studies, baroclinic instabilities formed periodically in the vicinity of the outflow source and predominantly on the downslope side of the current. Once the instabilities reach large amplitude, they caused the current to break up into a series of coherent subplumes spaced at intervals of 8–$12R_{\mathrm{d}}$, where

$$R_{\mathrm{d}} = \frac{[g(\rho_{\mathrm{p}} - \rho_{\mathrm{e}})B/\rho_{\mathrm{r}}]^{1/2}}{f} \tag{15}$$

is the Rossby radius of deformation based on the current height and f is the Coriolis parameter. As these structures move in the downstream direction we anticipate that rotationally dominated eddying motions will evolve across the whole width of the current owing to both continued baroclinic instability and eddy interactions (Griffiths et al., 1982; Griffiths and Linden, 1982; Griffiths and Hopfinger, 1984; Griffiths, 1986; Swaters, 1998). Following Griffiths and Hopfinger (1984) we then model the lateral expansion of the current as a (turbulent) diffusive process with the diffusion coefficient

$$\chi = \frac{1}{2}\frac{\mathrm{d}R^2}{\mathrm{d}t} = c_2 U_{\mathrm{rms}} \ell, \tag{16}$$

where $c_2 \approx 0.14$ is a constant (note this is a corrected value from that given by Griffiths and Hopfinger, 1984) and $\ell \approx 14R_{\mathrm{d}}$ is the lengthscale characterizing the eddy-like structures. Note that (16) describes the lateral expansion relative to the centreline of the current. Hence superposition of the mean descent rate of the current (4) on (16) will lead to an asymmetry between upslope and downslope expansion in the slope frame of reference (cf. Swaters, 1991; Jiang and Garwood, 1996; Swaters, 1998; Etling et al., 2000; Choboter and Swaters, 2000). We take the velocity scale characterizing the rotationally controlled turbulence to be $U_{\mathrm{rms}} = 0.3[g(\rho_{\mathrm{p}} - \rho_{\mathrm{e}})B/\rho_{\mathrm{r}}]^{1/2}$ (Griffiths and Hopfinger, 1984), and substituting for U_{rms}, ℓ and R_{d} in (16) gives

$$W_{\mathrm{p}}\frac{\mathrm{d}R^2}{\mathrm{d}z} = \frac{c_3}{f}\frac{g(\rho_{\mathrm{p}} - \rho_{\mathrm{e}})}{\rho_{\mathrm{r}}}B, \tag{17}$$

where the constant $c_3 \approx 1.2$. The current thickness B and half-width R represent a rectangular box approximation to the cross-stream thickness profile. The actual averaged path width of a meandering current may be much larger (and the depth smaller) as a result of eddies and meanders having scales comparable to the current width.

2.3. The interior flow

Continuity requires that the volume flux V carried downward in the slope current through any level z balances that upwelled in the basin interior (Baines and Turner, 1969), and this may be expressed as

$$V = \frac{\sqrt{\pi}BRW_{\mathrm{p}}}{\sin\theta} = -AW_{\mathrm{e}}. \tag{18}$$

Note that the factor of $\sin\theta$ is required to give the horizontal area in the current over which downwelling occurs. We also apply the advection–diffusion balance,

$$W_e \frac{d\rho_e}{dz} = \overline{\kappa^*} \frac{d^2\rho_e}{dz^2}, \tag{19}$$

in the interior of the basin. Here, W_e is the upwelling velocity and, following previous ocean models, we assume a uniform vertical diffusivity $\overline{\kappa^*}$. We ensure that there is no net heating of the ocean by applying at the surface ($z = 0$) the boundary condition

$$q_h = -\frac{c_p}{\alpha} \overline{\kappa^*} \frac{d\rho_e}{dz} A, \tag{20}$$

where c_p is the specific heat and α is the coefficient of thermal expansion. A different diffusivity in the surface boundary layer would have minimal effect on our solution since we are describing the circulation in terms of the heat flux carried by the flow, and therefore the diffusivity in the boundary layer will influence only the near-surface density gradient.

The buoyancy flux carried by the slope current through any level z is given by

$$F(z) = \int_{A_p(s)} g(\rho_p - \rho_e) U \, dA_p = \sqrt{\frac{\pi}{2}} \frac{BRW_p}{\sin\theta} g(\rho_p - \rho_e), \tag{21}$$

where $A_p(s)$ represents the current/plume cross-section. The upward diffusive flux in the interior must balance the buoyancy flux $F(z)$ in the slope current at every level,

$$F(z) = g\overline{\kappa^*} A \frac{d\rho_e}{dz}. \tag{22}$$

The plume volume flux V is given by (18) and the volume flux per unit depth entrained into the plume at any level is

$$Q = \frac{2RE_z W_p}{\sin\theta}. \tag{23}$$

2.4. The model system of equations

At the surface we require the volume and momentum fluxes in the slope current to be zero (cf. Baines and Turner, 1969). The buoyancy flux in the slope current at the surface is

$$F(0) = F_0 = \frac{\alpha g q_c}{c_p}, \tag{24}$$

where $q_c = -q_h$ is given by (20). At the bottom of the basin, the density anomaly approaches zero (and, therefore, the buoyancy flux $F(H)$ approaches zero in both the current and the interior). We check a posteriori that this condition is fulfilled by the solution. As in the "filling box" solution (Baines and Turner, 1969) the formulation does not represent the horizontal outflow from the slope current to the interior, which would require a horizontal density difference at the bottom.

The system of equations, (12)–(14) and (17)–(19), may be combined and integrated to give a third order system

$$\frac{dV}{dz} = Q, \tag{25}$$

$$\frac{dF}{dz} = -\frac{FV}{A\overline{\kappa^*}}, \tag{26}$$

and

$$R\frac{\mathrm{d}R}{\mathrm{d}z} = 2^{-1/4}c_1^{-1/2}c_3\pi^{-1/4}E_z^{1/2}\rho_\mathrm{r}^{-1/2}f^{-1}(\sin\theta)^{-1}\left(\frac{F}{Q}\right)^{1/2}, \tag{27}$$

where

$$Q = 2^{7/6}E_z\pi^{-1/6}c_1^{1/3}\rho_\mathrm{r}^{-1/3}F^{1/3}R^{2/3}. \tag{28}$$

Eqs. (25) and (26) describe respectively how the volume flux V and buoyancy flux F in both the interior and the slope current change with height owing to entrainment of ambient fluid from the interior into the current (at the rate Q given by (28)). Eq. (27) describes how the slope current half-width R increases with depth owing to both entrainment and baroclinic instability as it flows along the slope at an angle θ to the horizontal. These equations are based on the intimate connection between the slope current and the interior, and are solved numerically, whence the remaining quantities of interest may be calculated. The plume velocity and thickness are given by

$$W_\mathrm{p}^2 = \frac{2^{3/2}E_zc_1}{\sqrt{\pi}\rho_\mathrm{r}}\frac{F}{Q}\sin^2\theta, \tag{29}$$

and

$$B = \frac{2E_z}{\sqrt{\pi}}\frac{V}{Q}, \tag{30}$$

respectively, and the plume density by (21). The upwelling velocity and density profile in the interior, W_e and ρ_e, are found from (18) and (22), respectively. In particular, the solution provides a value for the total overturning volume flux $V_\mathrm{max} = V(H)$ and the top-to-bottom density difference $\Delta\rho = \rho_\mathrm{e}(H) - \rho_\mathrm{e}(0)$ in terms of the free parameter $\overline{\kappa^*}$.

3. Solutions and comparison with observations

For the purposes of applying the recycling box model in Section 2 to the global oceans we first consider the solution obtained for best estimates of theoretical and measured quantities, and two values of the diffusivity $\overline{\kappa^*}$. Thus we impose a surface cooling flux q_c equal to the poleward heat flux that is carried by the surface waters of the southern hemisphere (2×10^{15} W, Houghton et al., 1996, p. 212) and that drives bottom water formation. The bottom water is assumed to descend from the surface in slope currents that make an angle $\theta \approx 0.1°$ with the horizontal all the way to the bottom. This angle determines the distance that the slope current travels but has little effect on the total entrainment, as discussed in Section 2. As the model flow is two-dimensional (apart from the bottom water plume) we apply the matching heating flux $q_\mathrm{h} = -q_\mathrm{c}$ over the surface area of the global oceans $A = 3.6\times10^{14}$ m^2. We have taken $H = 3780$ m as the average depth of the oceans (Gill, 1982), $\rho_\mathrm{r} \sim 1025$ kg/m^3, $c_p \approx 3990$ J/kg/K for seawater at 20 °C and atmospheric pressure (Gill, 1982) and $\alpha = 2.54\times10^{-5}$ K^{-1} for seawater at −2 °C (Gill, 1982; this temperature being representative of the water in the Weddell Sea that feeds the sinking plumes and eventually becomes bottom water, Price and Baringer, 1994). The Coriolis parameter f is set to

1.37×10^{-4} rad/s, which corresponds to a latitude of 70°S. We examine the consistency between the conceptual model and ocean measurements without expecting solutions to be accurate in all respects.

Both the thermal boundary layer depth and the density difference between the surface and deep oceans are well predicted using the background diffusivity $\overline{\kappa^*} = 10^{-5}$ m^2/s measured in the open ocean (Fig. 3). The knee of the predicted density profile (or base of the thermocline) is sharper than the observed profiles. The deep oceans are predicted to be stratified, but it is apparent from profiles of the buoyancy frequency N (Fig. 4) that the predicted abyssal stratification is too weak. However, these differences are likely to result from the neglect of a number of factors. Ekman pumping in the upper ocean deepens the subtropical thermocline and shallows the subpolar thermocline, spreading the knee in the global average. Processes such as the formation of MODE waters and the model approximations for shallow depths, discussed earlier, are expected to influence the shape of the

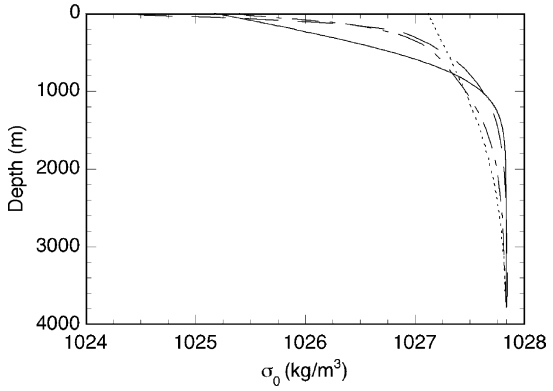

Fig. 3. Comparison of density profiles predicted by the recycling box model (for values of $\overline{\kappa^*} = 10^{-5}$, —, and 10^{-4} m^2/s, - - -) with potential density (σ_0) profiles averaged from the Levitus 1994 dataset (http://iridl.ldeo.columbia.edu/SOURCES/.LEVITUS94/) for the northern (— —) and southern (— - —) hemisphere oceans. The predicted density profiles are referenced to the global average potential density measured below depths of 3000 m (≈1027.83 kg/m^3).

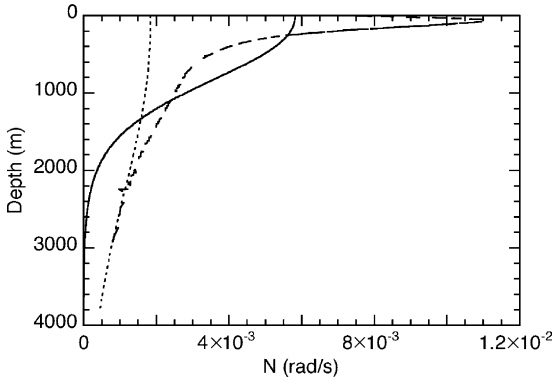

Fig. 4. Comparison of the buoyancy frequency profile in the oceans (dashed line) with that predicted by the recycling box model for $\overline{\kappa^*} = 10^{-5}$ m^2/s (solid line) and $\overline{\kappa^*} = 10^{-4}$ m^2/s (dotted line). The ocean data is a global mean and is taken from Peixoto and Oort (1992, p. 197).

profile through the thermocline. At abyssal depths, the unrealistically weak predicted stratification is the result of the density anomaly $\rho_p - \rho_e$ in the model being required to approach zero at the bottom, a requirement that leads to vanishing advective buoyancy flux (21) and, in turn, a vanishing diffusive buoyancy flux (and hence a vanishing gradient, (22)) in the interior. Temporal variations of the buoyancy flux in the "dominant" slope current (e.g. Fahrbach et al., 2001; Foldvik et al., 2004) and the division of sinking between several sites in the southern hemisphere will also lead to lateral intrusion over a range of depths. Additional sinking at sites in the northern hemisphere to form NADW also may influence the abyssal ocean stratification. In sharp contrast to the good agreement for $\overline{\kappa^*} = 10^{-5}$ m^2/s, the density profile predicted for $\overline{\kappa^*} = 10^{-4}$ m^2/s (a value typical of previous models) does not match observations, with a thermal boundary layer that extends through most of the depth and a small surface-to-bottom density difference. In this case the solution reproduces the measured density gradient at abyssal depths (Fig. 4).

The predicted width, thickness, along-stream velocity and density of the slope current are shown in Figs. 5 and 6. At a depth of 1000 m, the current thickness, speed and density anomaly ($\approx$150 m, 0.7 m/s and 0.3 kg/m^3, respectively) is consistent with values found to characterize the Filchner Shelf outflow into the Weddell Sea (100 m, 0.39 m/s and 0.08 kg/m^3, respectively; Price and Baringer, 1994). The predictions in Figs. 5 and 6 are also supported by hydrographic data at two downstream sections. At the first section, Foldvik et al. (2004) found an unsteady current centred at a depth of 1500 m that, when present, was approximately 50 km wide, more than 200 m thick and characterized by speeds of O(0.2) m/s (observations range between 0.16 and 0.5 m/s) and a potential temperature anomaly of about -1.5 °C (a potential density difference of O(0.04) kg/m^3) relative to the basin interior. At the second downstream section, Fahrbach et al. (2001) found the bottom water current at depths between about 1250 and 3000 m in a region approximately 250 km in width and 250 m thick (cf. Fig. 5). The average current speed was approximately 0.035 m/s and the potential temperature anomaly was of O(-0.6) °C (cf. Fig. 6). At times two cold cores were observed in the section, which is consistent with the cross-stream eddying structure assumed in our model in Section 2. The current height is predicted to increase very sharply below about 2000 m depth (Fig. 5). Although the large values of B become unrealistic

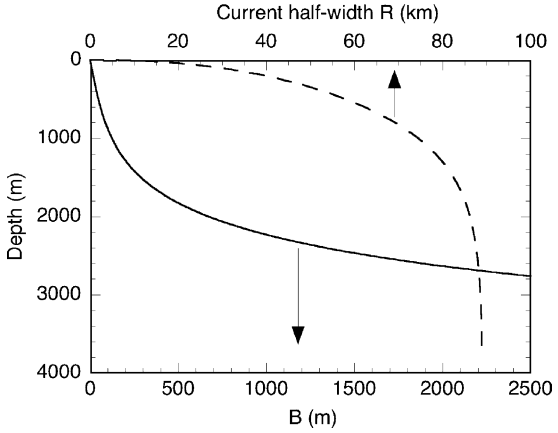

Fig. 5. Predictions of the steady-state recycling box model for the slope current thickness (solid line) and half-width (dashed line) for $\overline{\kappa^*} = 10^{-5}$ m^2/s.

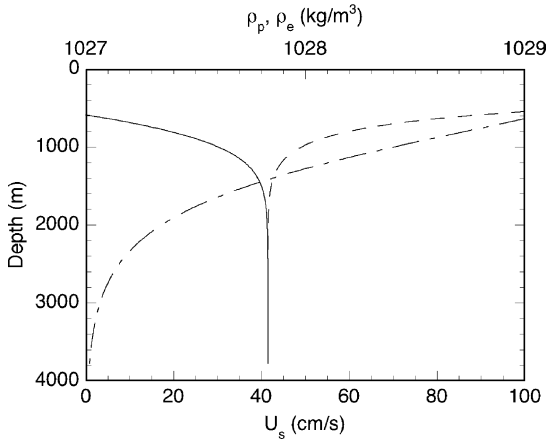

Fig. 6. Predictions of the steady-state recycling box model for the slope current speed (— - —) and the densities of the slope current (- - -) and the basin interior (—) for $\overline{\kappa^*} = 10^{-5}$ m^2/s. The predicted density profiles are referenced to the global average potential density measured below depths of 3000 m (≈1027.83 kg/m^3).

in this region (Fig. 6), the increase is a result of the density anomaly in the model being required to approach zero (as discussed in Section 2.4) in the absence of a representation of the horizontal outflow from the slope current to the interior. The plume volume flux must be maintained to the bottom, and without a density anomaly to maintain lateral spreading and current speed, the current thickness increases artificially.

Profiles of the upwelling velocity in the basin interior and entrainment flux into the slope current (Fig. 7) show for $\overline{\kappa^*} = 10^{-5}$ m^2/s that the upwelling velocity is almost uniform with depth at 0.5×10^{-7} m/s below 2000 m and that the entrainment flux peaks at 500 m and is negligible below

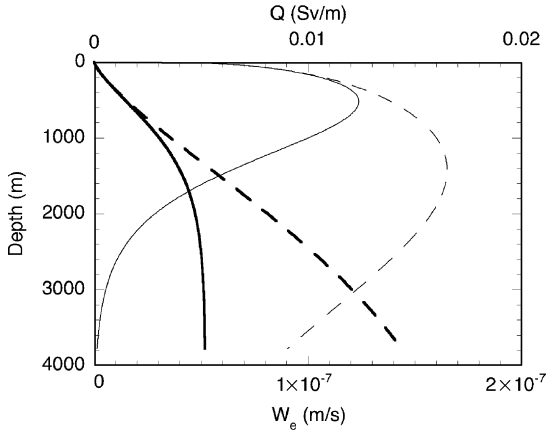

Fig. 7. Predictions of the steady-state recycling box model for the bulk upwelling velocity in the basin interior (bold lines) and the flux per unit depth entrained into the slope current (light lines). The solid and dashed lines correspond to predictions for $\overline{\kappa^*} = 10^{-5}$ and 10^{-4} m^2/s, respectively. The reference density ρ_r is taken to be 1025 kg/m^3 for seawater at 20 °C and atmospheric pressure (Gill, 1982). An upwelling velocity of 1×10^{-7} m/s over the area of the global ocean corresponds to a volume flux of 36 Sv (1 Sv = 10^6 m^3/s).

3000 m (where the current is unrealistically thick). In contrast, the upwelling velocity increases strongly with depth for $\overline{\kappa^*} = 10^{-4}\,\mathrm{m^2/s}$ and the entrainment flux into the plume remains large all the way to the bottom. The upwelling velocity predicted for $\overline{\kappa^*} = 10^{-5}\,\mathrm{m^2/s}$ is in good agreement with values (O(10^{-7}) m/s) inferred from radiocarbon and hydrographic data (Munk, 1966; Ganachaud and Wunsch, 2000; Ganachaud, 2003) for the deep oceans (above levels where the confining effect of bathymetry on water masses is relatively important). Chlorofluorocarbon (CFC) evidence from the Pacific thermocline (Matear and Wong, 1997) also supports upwelling velocities (1.5×10^{-8} m/s) and rates of diffusion ($1.5 \times 10^{-5}\,\mathrm{m^2/s}$ below the mixed-layer, and increasing with depth) that are comparable with our predictions for depths of 300 m. Below depths of 1000 m, we predict for $\overline{\kappa^*} = 10^{-5}\,\mathrm{m^2/s}$ that approximately 8 Sv of ambient water is entrained into the slope current (Fig. 7), in excellent agreement with the 7.4 ± 2.4 Sv obtained from a CFC inventory for the southern hemisphere (including, for a meaningful comparison, that flux recycled through the current at depth, see Fig. 5 of Orsi et al., 2002). Price and Baringer (1994) found in their model for the slope current in the Weddell Sea that most of the entrainment of ambient water occurred at depths between 700 and 1200 m, which we also predict for $\overline{\kappa^*} = 10^{-5}\,\mathrm{m^2/s}$ (Fig. 7, neglecting the region above the current starting depth of 700 m). This agreement is intriguing since Price and Baringer (1994) attribute the sudden entrainment to the acceleration of the current down a steepening topographic slope, which is an effect not included in our model. Moreover, our model suggests that entrainment flux per unit vertical distance is relatively insensitive to topographic slope (as seen in (11)).

The lack of consensus in the existing literature on overturning volume fluxes and rates of bottom water formation in the global oceans makes a comparison with our predictions challenging, in part because the global overturning circulation is likely to differ from the simple form assumed in this and many previous studies (e.g. see Sloyan and Rintoul, 2001). However, in attempting to place our own results in context we offer an interpretation that goes some way towards reconciling previous findings. Consequently we find that our predictions are not inconsistent with a number of previous studies, which have used a wide range of approaches. Munk and Wunsch (1998) argue for an average upwelling flux through the deep and abyssal oceans of approximately 30 Sv, which corresponds to a timescale of O(1500) years for the replacement of the total ocean volume (assumed to be comparable with the oldest water mass mixture in the ocean, England, 1995). Remarkably, if we multiply our predicted upwelling velocity at the ocean bottom (Fig. 7) by the cross-sectional area A we obtain 18.4 Sv of interior upwelling/overturning. Given that bottom waters are produced in the southern hemisphere (as AABW, which is typically characterized by potential temperatures less than 0 °C or the neutral density surfaces $\gamma^n > 28.27\,\mathrm{kg/m^3}$, e.g. see Orsi et al., 2002), this prediction is also consistent with those from the hydrographic inversions of Ganachaud and Wunsch (2000) and Ganachaud (2003) (21 ± 6 Sv in the Southern Ocean) and Sloyan and Rintoul (2001) (27 Sv injection into the bottom waters).

Our predictions (Fig. 7) agree with observations (Price and Baringer, 1994; Weppernig et al., 1996; Fahrbach et al., 2001; Foldvik et al., 2004) that entrainment results in a bottom water formation rate 2–3 times greater than the volume flux of source water supplying the slope current (the source in the Weddell Sea is Ice Shelf Water from the Filchner Depression at about 600 m depth, e.g. Foldvik et al., 2004). However, these studies have suggested smaller absolute rates of bottom water formation around Antarctica. Field observations of the bottom water plume in the northwestern Weddell Sea (Fahrbach et al., 2001) gave a bottom water formation rate of

1.3 ± 0.4 Sv, which compares with 2.2 Sv predicted by the model of Price and Baringer (1994). The identification of several plumes in the Weddell Sea (Foldvik et al., 2004) leads to larger estimates for the Weddell Sea Bottom Water (WSBW, characterized by potential temperatures less than -0.7 °C, e.g. see Fahrbach et al., 2001) formation rate of about 5 Sv (Weppernig et al., 1996; Foldvik et al., 2004). These volume fluxes, though still relatively small, are augmented by entrainment of overlying Weddell Deep Sea Water (WSDW) as WSBW exits the Weddell Sea and becomes AABW (Mensch et al., 1996, finds 11 Sv of AABW to be derived from 3.5 Sv of new WSBW). Although the majority of AABW is thought to have its origins in the Weddell Sea (e.g. Price and Baringer, 1994; Orsi et al., 1999), additional contributions come from several other sites around Antarctica (e.g. Sloyan and Rintoul, 2001).

Studies of transient tracer redistribution offer a means of estimating the total bottom water formation rate. CFC and tritium inventories in the southern hemisphere have given fluxes of 8–9.5 Sv (Orsi et al., 1999), 8.1 ± 2.6 Sv (Orsi et al., 2002) and at least 14 Sv (Mensch et al., 1996). We note that these values are not necessarily inconsistent with the predictions of our model and previous hydrographic inverse box models. Unsteady buoyancy forcing at the ocean surface gives rise to temporal variations in the slope current (Fahrbach et al., 2001; Foldvik et al., 2004). Bottom water formation will only occur when the buoyancy flux is large, while water in the slope current does not reach the bottom at other times and instead enters the basin interior at a shallower depth (Killworth and Turner, 1982). The CFC tracer distribution confirms this behaviour with 9.4 Sv estimated to enter the deep interior (i.e. as Modified Circumpolar Deep Water rather than as AABW) from the sinking regions in the southern hemisphere (Orsi et al., 2002). This contribution brings the total deep and bottom water formation rate to 17.2 Sv (which, for a meaningful comparison, includes that flux recycled through the slope current at depth). This is significantly closer to our prediction based on steady surface heat fluxes, and suggests that the agreement could be improved by incorporating unsteadiness into our model. As noted by Sloyan and Rintoul (2001), bottom water formation rates computed from hydrographic inverse box models include the flux entrained from overlying waters after the bottom water leaves the slope current and circulates through the box. Therefore, we expect such formation rates to be larger than the bottom water formation rate defined in this study in terms of the volume flux in the slope current.

In summary, the data interpretations are consistent with southern hemisphere plumes that replenish abyssal waters at a rate in the vicinity of 10–30 Sv. Approximately 3.6 Sv (Fig. 7) is predicted to be transported upward into the thermal boundary layer (at approximately 400 m depth, Fig. 3) and this is the net southward volume flux predicted within the thermocline.

4. Parameter dependence and sensitivity analysis

In order to explore the solution dependence on the key variables q_c and $\overline{\kappa^*}$, and the sensitivity of the solution to uncertainties in a number of coefficients for parameterized processes, we vary one quantity at a time, keeping all others fixed at the "preferred" values discussed above. The results can be compared (see Table 1) with related predictions of the non-rotating boundary layer scaling analysis of Rossby (1965), which was extended to the case of an applied flux by Mullarney et al. (2004), and with the geostrophic boundary layer scaling proposed for the ocean by Bryan and Cox

Table 1
Summary of power laws obtained from the results of the recycling box model, from the scalings based on non-rotating (Rossby, 1965; Mullarney et al., 2004) and geostrophic theories (Bryan and Cox, 1967; Park and Whitehead, 1999), and from GCM studies (Park and Bryan, 2001)[a]

	Recycling box	Non-rotating	Geostrophic	GCMs
Applied flux:				
$\Delta T \sim$	$E_z^{-0.4}\overline{\kappa^*}^{-0.56} q_c^{4/5}$	$\overline{\kappa^*}^{-2/3} q_c^{5/6}$	$\overline{\kappa^*}^{-1/2} q_c^{3/4}$	
$V_{\max} \sim$	$E_z^{0.45}\overline{\kappa^*}^{0.56} q_c^{1/5}$	$\overline{\kappa^*}^{2/3} q_c^{1/6}$	$\overline{\kappa^*}^{1/2} q_c^{1/4}$	
$\delta \sim$	$E_z^{-0.43}\overline{\kappa^*}^{0.4} q_c^{-1/5}$	$\overline{\kappa^*}^{1/3} q_c^{-1/6}$	$\overline{\kappa^*}^{1/2} q_c^{-1/4}$	
Applied ΔT:				
$q_c \sim$	$E_z^{0.50}\overline{\kappa^*}^{0.70} \Delta T^{5/4}$	$\overline{\kappa^*}^{4/5} \Delta T^{6/5}$	$\overline{\kappa^*}^{2/3} \Delta T^{4/3}$	$\overline{\kappa^*}^{0.57-0.67}$
$V_{\max}$	$E_z^{0.56}\overline{\kappa^*}^{0.70} \Delta T^{1/4}$	$\overline{\kappa^*}^{4/5} \Delta T^{1/5}$	$\overline{\kappa^*}^{2/3} \Delta T^{1/3}$	$\overline{\kappa^*}^{0.45-0.6}$
$\delta \sim$	$E_z^{-0.53}\overline{\kappa^*}^{0.25} \Delta T^{-1/4}$	$\overline{\kappa^*}^{1/5} \Delta T^{-1/5}$	$\overline{\kappa^*}^{1/3} \Delta T^{-1/3}$	$\overline{\kappa^*}^{0.34-0.38}$

[a] Note that no GCM results are available for the case of an applied boundary flux. See text for the derivation of the recycling box results.

(1967), and extended to the case of an applied flux by Park and Whitehead (1999). We also compare with a number of GCM results, particularly those of Park and Bryan (2000).

Fig. 8 shows the predicted overturning volume flux $V_{\max} = V(H)$, the top-to-bottom density difference $\Delta\rho = \sigma_0(H) - \sigma_0(0)$ and the surface boundary layer thickness δ as functions of the surface buoyancy flux $F_0 = g\alpha q_c/\rho c_p$. In the case of the strongest sinking, $V_{\max}$ is also the rate of formation of bottom water. The boundary layer thickness is defined as the depth δ below the surface at which the density difference $\sigma_0(H) - \sigma_0(\delta)$ falls to $1/e$ of the top-to-bottom difference. The estimated heat transport of 2 PW in each hemisphere (with thermal expansion coefficient $\alpha = 2.54 \times 10^{-5}\ \mathrm{K}^{-1}$) corresponds to a buoyancy flux of 1.2×10^5 N/s. The predicted volume flux power law $V_{\max} \sim q_c^{1/5}$ has an exponent between the non-rotating scaling $V_{\max} \sim q_c^{1/6}$ and the geostrophic scaling law $V_{\max} \sim q_c^{1/4}$. The predicted density difference varies as $q_c^{4/5}$, which again lies between the non-rotating $\Delta\rho \sim q_c^{5/6}$ and the geostrophic $\Delta\rho \sim q_c^{3/4}$ scaling laws. The boundary layer thickness is predicted to vary as $q_c^{-1/5}$, and this too lies between the non-rotating and geostrophic scalings $\delta \sim q_c^{-1/6}$ and $\delta \sim q_c^{-1/4}$, respectively.

The measured global average ocean values for $\Delta\rho$ and δ are shown in Fig. 8 as a band extending between the averages of that quantity for the northern and southern hemispheres. For $V_{\max}$ the band shows the range of estimates discussed in Section 3. Of these quantities the observed top-to-bottom density difference provides the tightest constraint on the applied buoyancy flux for which the model matches observations: for the "preferred" values of all other quantities, a heat flux of 2 PW accurately predicts the density difference. The actual overturning volume flux is much more uncertain (as discussed earlier) and can accommodate a wide range of model heat fluxes. The measured e-folding depth for density (150 m and 320 m in the Southern and Northern hemispheres, respectively) indicates that the average ocean thermocline depth is significantly shallower than the 520 m predicted for the model thermal boundary layer. Comparisons using either the e-folding depth for buoyancy frequency or a knee in the profile of buoyancy frequency lead to a similar conclusion. The shallower ocean thermocline might be a result of Ekman pumping, which tends to deepen the thermocline in the subtropics and western regions of basins, and to make it shallower at

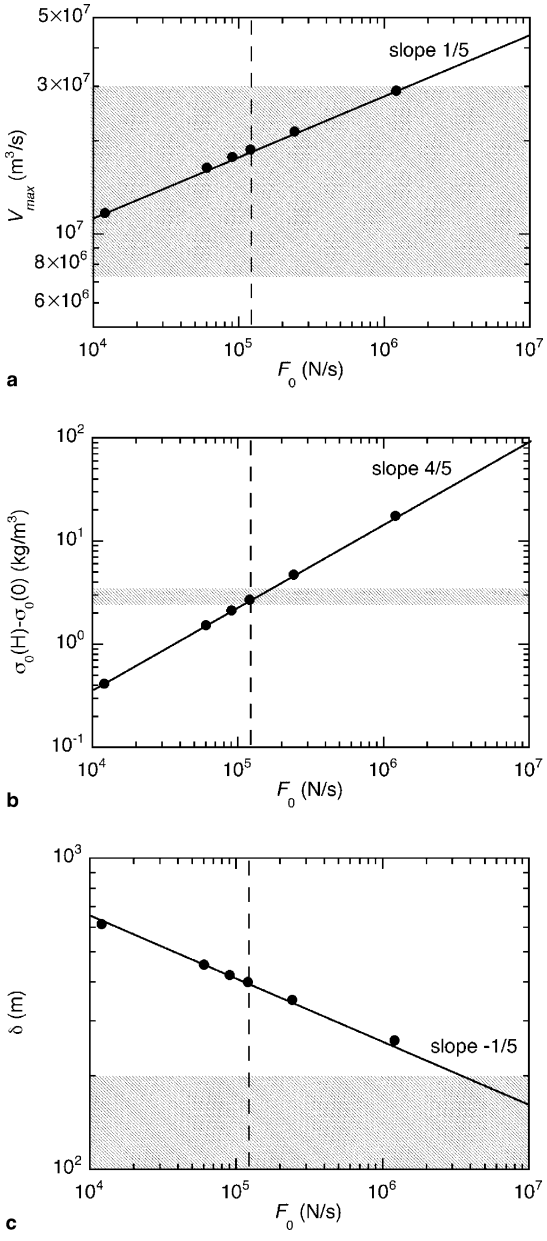

Fig. 8. The theoretical dependence of (a) overturning volume flux, (b) top-to-bottom density difference and (c) boundary layer thickness on the applied buoyancy (heat) flux, for "preferred" values of all other quantities. The hatched band indicates the uncertainty of the measured globally-averaged ocean value in each case. Lines indicate the rational power law slopes that fit the data. The vertical line indicates the observed heat flux of 2 PW.

high latitudes and eastern regions, thus broadening the curvature of the hemisphere-averaged density profiles. Our neglect of wind stress and planetary vorticity effects is expected to make the boundary layer depth the least accurate of our comparisons, but nonetheless an interesting result.

Fig. 9 shows the same predicted volume flux, top-to-bottom density difference and boundary layer thickness as in Fig. 8, but as functions of the interior vertical diffusivity $\overline{\kappa^*}$ (with $q_c = 2$ PW and $\alpha = 2.54 \times 10^{-5}\ \mathrm{K}^{-1}$). The predicted volume flux follows a power law $V_{\max} \sim \overline{\kappa^*}^{0.56}$, a slightly

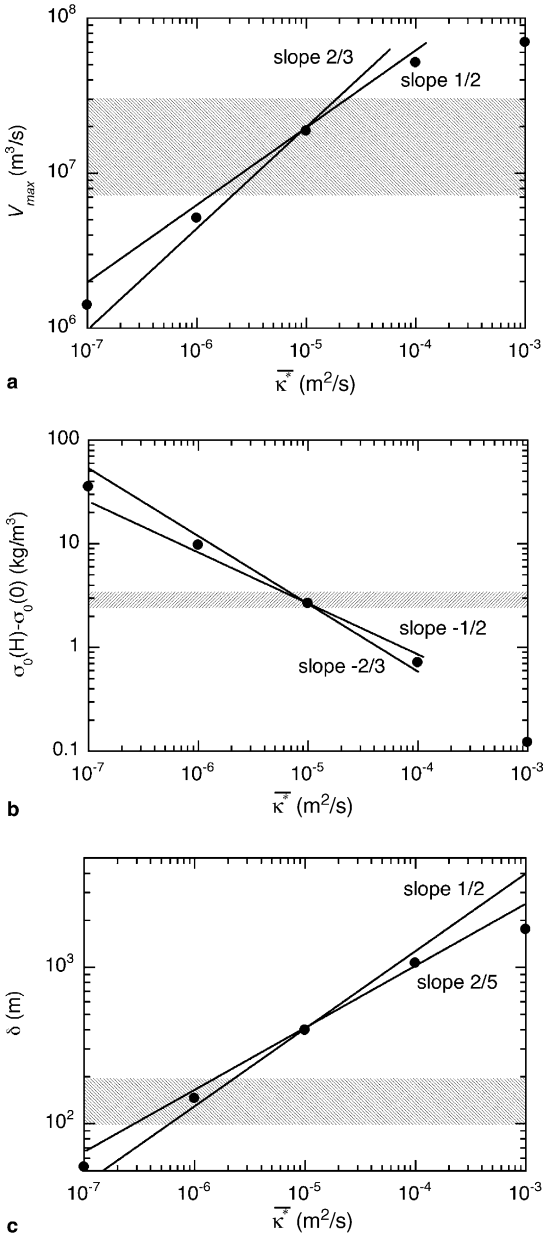

Fig. 9. The theoretical dependence of (a) overturning volume flux, (b) top-to-bottom density difference and (c) boundary layer thickness on the interior vertical diffusivity, for "preferred" values of all other quantities. The hatched band indicates the uncertainty of the measured globally-averaged ocean value in each case. Lines indicate the power law slopes predicted by the non-rotating and geostrophic scaling theories (Table 1).

weaker dependence than the non-rotating scaling $V_{\max} \sim \overline{\kappa^*}^{2/3}$ and slightly stronger dependence than the geostrophic scaling result $V_{\max} \sim \overline{\kappa^*}^{1/2}$. The predicted density difference varies as $\overline{\kappa^*}^{-0.56}$, and this again lies between the non-rotating ($\overline{\kappa^*}^{-2/3}$) and geostrophic ($\overline{\kappa^*}^{-1/2}$) scaling. The boundary layer thickness varies with $\overline{\kappa^*}^{0.40}$, again intermediate to the non-rotating and geostrophic scalings, $\delta \sim \overline{\kappa^*}^{1/3}$ and $\overline{\kappa^*}^{1/2}$, respectively. Comparison with ocean values shows again that the density difference is well predicted only by $\overline{\kappa^*} = 10^{-5}$ m^2/s. The variation of volume flux with $\overline{\kappa^*}$ is sufficiently rapid that even the broad uncertainty in the ocean overturning rate permits only moderate diffusivities. The predicted average thermocline depth, for all but extremely small diffusivities, is again larger than that measured in the oceans.

If entrainment plays a significant role in the overturning then we expect a strong dependence of key observables on the entrainment constant E_z. Solutions using $E_z = 0.05$, 0.1 and 0.2 (Fig. 10) are well fitted by the power laws $V_{\max} \sim E_z^{0.45}, \Delta\rho \sim E_z^{-0.4}$ and $\delta \sim E_z^{-0.43}$. Thus increasing the entrainment rates increases overturning rate (as defined by the plume or bottom water volume flux) and decreases density differences, but also decreases the boundary layer thickness. All values of E_z in this range (with the "preferred" values of other quantities) provide consistency with the actual bottom water formation rate (12–25 Sv), whereas the largest value of the entrainment constant gives a density difference that is too small.

Other quantities that are assumed constant with depth and forcing strength in the theoretical formulation, and that have been held at fixed values in the above discussion, include three variables, along-current bottom slope θ, Coriolis parameter f and ocean area A, along with the semi-empirical coefficients $c_1 = 1$ (for the Froude number of the slope current, from (7)) and $c_3 = 1.2$ (relating lateral spreading of the slope current to baroclinic eddy properties, from (17)). Solutions were obtained at larger and smaller values of each. For example, increasing bottom slope by a factor of five decreases the overturning volume flux by 20% and increases the top-to-bottom density difference by 20%. Decreasing A by 40% to match the real ocean area at a depth of 4000 m increases the upwelling velocity by 27%, slightly thins the boundary layer and decreases the overturning rate by 21%. Decreasing f to that appropriate to latitude 20° increases the overturning by 15%. Increasing c_1 by a factor of two (considered to be an outer bound) increases $V_{\max}$ by 5% and decreases the density difference by 5%. Increasing c_3 by a factor of two increases $V_{\max}$ by 8% and decreases density difference by 8%. We conclude that these variables and constants all describe aspects of the flow that are of some significance in governing the overturning circulation of the model. At the same time, the uncertainties in the appropriate values and the sensitivity of the results to these quantities are small enough to make the calculations reliable and robust. The robustness is particularly well demonstrated by a version of the model in which sinking is modelled as a simple turbulent plume falling vertically to the ocean bottom, in place of the slope current, and for which the results using the "preferred" input values in Section 3 are comparable ($V_{\max} \approx 9.4$ Sv, $\Delta\rho = 2.4$ kg/m^3 and $\delta \approx 600$ m). Note that if θ or E_z are allowed to vary with depth a more complicated set of equations must be solved. However, solutions with depth-dependent area A are readily obtained from (25)–(27). The ocean area decreases by only 10% from the surface to 2000 m, 25% to 3000 m, and 40% to 4000 m depth. This can lead to a modification of the depth-dependence of upwelling velocity and density. For the geometry in Fig. 1b, with $A(z)$ decreasing linearly from $A(0)$ to $A(H) = 0.6A(0)$, we find that the upwelling velocity at the bottom increases by 60%, but that the overturning flux decreases by only 5% and the top-to-bottom density difference is virtually unchanged.

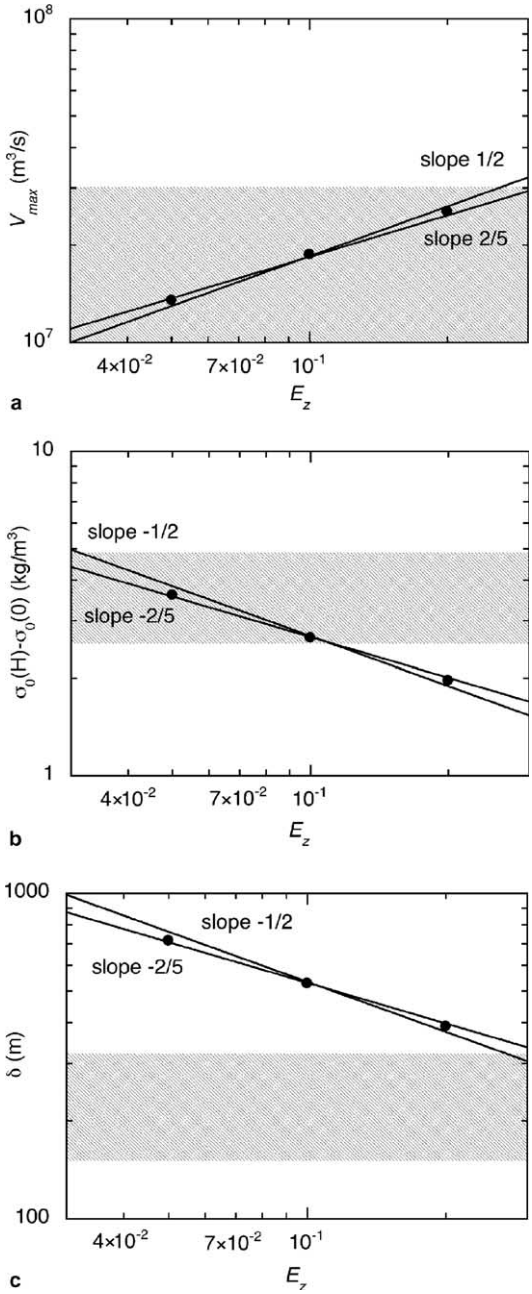

Fig. 10. The theoretical dependence of (a) overturning volume flux, (b) top-to-bottom density difference and (c) boundary layer thickness on the entrainment constant, for ''preferred'' values of all other quantities. The hatched band indicates the uncertainty of the measured globally-averaged ocean value in each case. Lines indicate the power law slopes predicted by the non-rotating and geostrophic scaling theories (Table 1).

When comparing the present results to previous GCM studies it should be remembered that power laws expressed in terms of heat flux differ from those expressed in terms of temperature difference. Most emphasis in GCMs has been on the calculated heat transport as a function of vertical diffusivity and applied temperature difference (with a restoring flux condition). Thus the slopes in Figs. 8 and 9 cannot be directly compared with previously reported power laws. In addition, the results of GCMs are not generally reported in the detail required for a full comparison with our results, and there are no GCM results available for comparison with the entrainment dependence of Fig. 10. However, Park and Bryan (2000) carried out a comparison of z-coordinate and isopycnal-coordinate GCMs, for a thermally-driven overturning and an overturning forced by both heating and wind stress, and reported the effects of varying the vertical diffusivity. Broadly, these GCM results (Table 1) are only slightly different from the trends predicted by geostrophic scaling and are therefore similar to the predictions of the theory presented here.

For a more detailed comparison we convert the present predictions into corresponding power laws for the case of an applied temperature difference, and assume the two simple (temperature and flux) boundary conditions place bounds on the behaviour expected under the restoring thermal boundary conditions typically used in GCMs. The results of Figs. 8–10, although based on changing only one variable at a time, can be approximated as

$$V_{\max} \sim E_z^{0.45}\overline{\kappa^*}^{0.56} q_c^{1/5}, \tag{31}$$

$$\Delta\rho \sim E_z^{-0.4}\overline{\kappa^*}^{-0.56} q_c^{4/5}, \tag{32}$$

$$\delta \sim E_z^{-0.43}\overline{\kappa^*}^{0.4} q_c^{-1/5}, \tag{33}$$

and can be rearranged to give the dependence for an applied density difference $\Delta\rho$ (repeated in Table 1):

$$q_c \sim E_z^{0.50}\overline{\kappa^*}^{0.70} \Delta\rho^{5/4}, \tag{34}$$

$$V_{\max} \sim E_z^{0.56}\overline{\kappa^*}^{0.70} \Delta\rho^{1/4}, \tag{35}$$

$$\delta \sim E_z^{-0.53}\overline{\kappa^*}^{0.25} \Delta\rho^{-1/4}. \tag{36}$$

These predicted power laws for q_c, $V_{\max}$ and δ for an applied temperature difference again fall between the non-rotating (Rossby, 1965) and geostrophic (Bryan and Cox, 1967) boundary layer scaling laws, although those scalings have nothing to say about the effect of entrainment. For boundary layer depth, these scaling theories give $\delta \sim \overline{\kappa^*}^{1/5}$ and $\delta \sim \overline{\kappa^*}^{1/3}$, respectively. The GCM results of Park and Bryan (2000) are described by the approximate power laws

$$q_c \sim \overline{\kappa^*}^{0.57-0.67}, \tag{37}$$

$$V_{\max} \sim \overline{\kappa^*}^{0.45-0.6}, \tag{38}$$

$$\delta \sim \overline{\kappa^*}^{0.34-0.38}, \tag{39}$$

where dependence on temperature difference was not reported and the larger powers in the ranges shown for q_c and $V_{\max}$ were found using in situ rather than imposed restoring density differences to estimate the geostrophic velocity. There was little difference between results for flat bottom and bowl shaped basins, only minor differences between the z-coordinate and isopycnal layered models, and only a small (at $\overline{\kappa^*} > 10^{-5}$ m^2/s) increase of heat flux when wind stress was applied. Several

earlier GCM studies collated by Park and Bryan (2000) gave a heat flux dependence $q_c \sim \overline{\kappa^*}^{0.54-0.58}$. The larger powers in (37) and (38) are only slightly smaller (or slightly larger in the case of δ) than those predicted by the simple geostrophic scaling, whereas our recycling box model implies powers (34)–(36) for q_c and V_{max} slightly larger than the geostrophic scaling. The largest difference in behaviour is the relatively weak variation of boundary layer thickness with diffusivity (36) in the present model. This behaviour is consistent with the greater rates of entrainment into the sinking region for larger $\overline{\kappa^*}$, which leads to more recycling at depth and less variation of the boundary layer thickness. Note that the recycling box model and GCMs consider the dynamics of the whole volume, whereas the scaling analyses consider only the dynamics of the upper boundary layer.

The theoretical model can also be compared to GCMs in terms of the predicted magnitudes for key dependent variables. As discussed in Section 3, the recycling box model compares well with the observed ocean (apart from a larger predicted thermocline thickness and weaker abyssal stratification) for a diffusivity of $10^{-5}\,m^2/s$, whereas GCM results tend to agree with ocean values when $\overline{\kappa^*}$ is set to the order of $10^{-4}\,m^2/s$. Thus the recycling box model gives an overturning rate for the present base set of "preferred" parameter values (including $\overline{\kappa^*} = 10^{-5}\,m^2/s$) of 20 Sv, approximately a factor of four larger than that computed by Park and Bryan (2000) for that diffusivity. Under these same conditions the boundary layer thickness given by the GCM is 150 m (defined at 30°N), whereas our model gives 400 m. The ocean temperature difference in the GCM was 22 °C (with expansion coefficient $\alpha = 2 \times 10^{-4}\,K^{-1}$), which equates to a density difference of $5.6\,kg/m^3$, nearly double the average density difference measured in the oceans and predicted by the present model.

The differences between GCM results and the theory are consistent with the expected effects of entrainment into the plume. The point here is that the calculations in Section 3 were based on reasonably well-constrained and previously established values for input variables and semi-empirical constants, and therefore represent our best estimates for the ocean. However, the predicted power law dependences (31)–(33) indicate that the observed ocean density difference and overturn rate can be achieved by selecting a range of suitable combinations of diffusivity and entrainment constant. For example, the same flow can be achieved with a larger diffusivity and a smaller entrainment (as is found when moving from the present model, with its explicit description of entrainment, to previous GCMs, which use larger $\overline{\kappa^*}$ but have little control of the effective rates of entrainment). However, in the present theory diffusivity and entrainment have opposing effects on boundary layer thickness, so that increasing one and decreasing the other greatly alters δ. This behaviour illustrates the effects of entrainment into the sinking region. For a diffusivity of $10^{-4}\,m^2/s$ (which requires $E_z = 0.02$ to give the observed density difference) we find a much larger boundary layer thickness (2000 m) than for $\overline{\kappa^*} \sim 10^{-5}\,m^2/s$ (for which the model requires $E_z = 0.1$ to match observations and gives $\delta = 400$ m). Thus our solution for the ocean based on "preferred" values is apparently close to the optimum that gives the best fit to observed $\Delta\rho$, V_{max} and δ. It is also consistent with GCM results if we assume these have a smaller rate of entrainment into sinking regions.

5. Discussion of vertical diffusivities

The application of a theoretical one-dimensional advection–diffusion balance to the measured abyssal gradients gives a larger diffusivity κ_m (e.g. Munk, 1966; Munk and Wunsch, 1998) than

the present theory. The addition to the Munk (1966) balance of entrainment into sinking regions (at least above 2500 m for the present slope plume model), and its fit to the measured stratification at 1000–3000 m, would require a diffusivity κ_e that is a factor of 2–3 less than κ_m by virtue of the depth-dependent upwelling velocity and associated convergence of isopycnals as water is upwelled. However, fitting of the Munk balance (or its modification to take account of entrainment) to the measured abyssal gradients does not take into account the way in which those gradients are linked to the surface fluxes (or, equivalently, to the top-to-bottom density difference). The present theory is an attempt to describe that link (albeit one that may be inaccurate in terms of the profile within the thermocline owing to the action of processes not represented in the theory, and also near the bottom owing to the neglect of the density difference required for a horizontal outflow). Hence the magnitude of κ_m is not easily related to the $\overline{\kappa^*}$ predicted by the recycling box theory.

The theory links the surface to the abyss by requiring that the flux of plume buoyancy delivered through any depth matches the interior diffusive flux through that depth. The plume buoyancy flux at its source is given by the surface heating (which we can think of as a known, fixed quantity) and the plume flux at any other depth is also determined by the plume dynamics and entrainment (these are coupled to the interior stratification, but let us consider that a secondary factor and therefore independent of interior diffusivity). The magnitude of the interior heat flux (which, incidentally, must be present in a steady state, no matter how much of the upwelling is wind-driven) must therefore also be set by these factors. Hence the interior gradients in both the thermocline and the abyss must be determined by the plume behaviour.

As it is difficult to directly compare κ_m and $\overline{\kappa^*}$, we instead illustrate the extreme sensitivity of the diffusivity $\overline{\kappa^*}$ to entrainment into the slope current, for the case where the surface heat fluxes are linked to the dynamics of the whole water column. Fig. 11 shows the diffusivity required in a recycling box model as the entrainment coefficient E_z is varied, while the top-to-bottom density difference $\Delta\rho$ and overturning flux V_{max} are held constant. The locus in E_z–$\overline{\kappa^*}$ space is calculated using (35) in the neighbourhood of the solution based on the "preferred" parameter values. Although

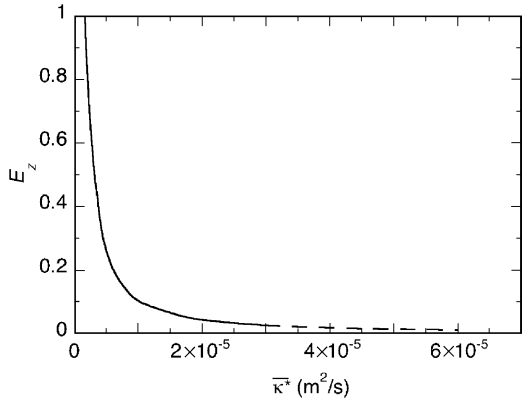

Fig. 11. Dependence upon E_z of the diffusivity required in the recycling box model with overturning flux V_{max} and top-to-bottom density difference $\Delta\rho$ held fixed. The locus is shown as a solid line in the neighbourhood of the "preferred" parameter values $E_z = 0.1$ and $\overline{\kappa^*} = 10^{-5}\ m^2/s$. For values of $\overline{\kappa^*} \gtrsim 3 \times 10^{-5}\ m^2/s$, the dotted line indicates that the entrainment constant becomes so small that the total flux entrained into the slope current can no longer reach V_{max}.

the power law becomes only approximate as the diffusivity increases (as indicated by the dotted line for $\overline{\kappa^*} \gtrsim 3 \times 10^{-5}$ m^2/s, where entrainment into the plume becomes so small that the volume flux is unable to reach $V_{\max}$), it is apparent that a small decrease in entrainment constant is compensated for by a large increase in interior diffusivity (this becoming necessary to maintain the prescribed $\Delta\rho$). This behaviour is therefore qualitatively consistent with a relatively small increase in volume flux entrained into the slope current between 1000 and 3000 m corresponding to a reduction of the required diffusivity by a much larger factor.

For $\overline{\kappa^*} = 10^{-5}$ m^2/s the predicted top-to-bottom density difference agrees well with observations. The interior structure in the density profile differs, and we appeal to thermocline processes and additional (northern hemisphere) sinking as the main explanations for this discrepancy. The heat fluxes required for additional sinking regions are assumed to be supplied in the northern hemisphere and have not been included in our calculation since the main density structure is determined by the bottom water plume (Killworth and Turner, 1982). The additional heat uptake required at the surface can be accommodated with an increase in the density gradient near the surface, which is consistent with the difference between the predictions and observations in Fig. 3. In the abyss, the weaker stratification is associated with the model formulation, which gives very thick slope currents owing to the vanishing density anomaly at the bottom.

Finally a comparison of this circulation model with the horizontal convection experiments of Mullarney et al. (2004) is successful but will be reported elsewhere as it requires reformulation of the plume model to describe a vertical line plume spanning the width of one end of the box.

6. Concluding remarks

A simple theoretical model has been developed to examine the magnitude of a convective meridional overturning circulation forced by the observed meridional heat transport of the oceans. The circulation is also assumed to be governed by a uniform rate of vertical mixing throughout the interior. The predicted convective overturning is expected to be one contribution to the overall global thermohaline circulation. Enhancement of the overturning by wind-forced upwelling in the Southern Ocean will further reduce the required vertical diffusivity and the energy requirements for mixing (Tsujino and Suginohara, 1999; Webb and Suginohara, 2001).

Entrainment into regions of turbulent downwelling is known to be an important process for the generation and maintenance of a density stratification in finite volumes of fluid. However, this process has effectively been neglected in previous discussions of the vertical advection–diffusion balance that maintains the deep density stratification in diffusive theories for the ocean overturning. Previous predictions of the external energy inputs required to maintain the deep density stratification against the interior upwelling velocity are based on a one-dimensional balance, whereas entrainment can withdraw water from the interior over a range of depths, inducing recirculation at depth and reducing the external energy requirement for mixing. Entrainment is not resolved by current hydrographic inversions. We propose that it occurs in bottom currents, which flow on gentle slopes, and that the previously reported (very small) along-current entrainment rates correspond to considerable rates of entrainment when expressed as inflow rates per unit depth of sinking. The potential significance of entrainment is evidenced by estimates of the large increase in volume flux with depth in slope currents. It is very difficult to

represent this entrainment accurately in numerical simulations of large-scale ocean circulation. In the model reported here we have not attempted to further refine the parameterization of turbulent entrainment, focusing instead on the effects of entrainment on the basin-scale and global overturning circulation.

Our analysis for the ocean interior flow does not explicitly describe the effects of planetary rotation, or the quasi-horizontal currents, gyres and eddies forced by wind stress or buoyancy. Indeed, we have no need to discuss a horizontal momentum equation or velocity field for the interior and surface boundary layer. We have instead solved for the vertical component of the interior flow, requiring only that the isopycnal surfaces in the interior, in a zonal average, are approximately horizontal except where they slope upwards and approach the surface owing to cooling. Effects of planetary rotation are included through use of the observed heat flux, which is treated as an imposed surface boundary condition. The role of surface wind stress is included to the extent that it may be responsible for heat transport, effectively imposing a heat flux on the vertical overturning. Freshwater and salinity buoyancy fluxes can in principle be included, but are smaller, of the order of only 10% of the thermal buoyancy flux. There is substantial benefit in considering the overturning forced by a prescribed heat flux (and governed by a prescribed vertical diffusivity). The model then predicts both the mass fluxes and the temperature (density) difference from top to bottom (which approximates the surface temperature difference from equator to pole). Of the 2 PW heat flux applied at the surface, the solution for $\kappa = 10^{-5}\,\mathrm{m^2/s}$ implies that approximately 0.5 PW pass through the abyssal flow (taking vertical diffusion or, equivalently, the plume buoyancy flux through a depth of 1000 m).

An additional complexity in the Southern Ocean is that some of the upwelling is thought to be wind-driven, in which case the overturning rate may be governed by a combination of convection, Ekman pumping and vertical mixing in the interior. Nevertheless, the vertical mixing in the abyssal waters remains essential to the maintenance of a horizontal density difference between sinking and interior waters, hence to the continued flow of dense waters to the bottom. Buoyancy forcing too remains essential if the sinking is to occur in localized regions, such as sill overflows and slope currents.

When applied to the oceans the convection model yields predictions that are consistent with a wide range of previous studies and field observations. This agreement supports the hypothesis that entrainment might play a key role not only in the dense slope currents, but also in the global overturning circulation. The results are also consistent with previously reported GCM studies, but indicate the somewhat similar effects on volume flux of larger entrainment and larger interior vertical diffusivity. We conclude that buoyancy forcing at the sea surface might be capable of driving a substantial fraction, and perhaps all, of the mass flux in the observed overturning circulation. This conclusion depends on the interior mixing rate, and hence on the rate of supply of energy to turbulence from winds, tides or buoyancy. An important conclusion is that rates of vertical mixing larger than measured in the oceans might not be required. Larger rates of mixing in the theory give unrealistically rapid overturning, a large thermocline depth and small top-to-bottom density differences.

Further improvements of the theory should focus on the bottom boundary condition and lateral spreading of the bottom water, on describing the overturning with two major sinking regions, on analyzing temporal responses to boundary conditions and on the effects of temperature-dependent thermal expansion in the non-linear equation of state.

Acknowledgments

We thank Stewart Turner, Trevor McDougall and James Ledwell for their helpful comments on earlier versions of this manuscript. During preparation of this article, we became aware of a steady "filling-box" model incorporating Eqs. (19)–(22) with sinking in a vertical turbulent plume and developed by William Peterson, to whom we are very grateful for providing a copy of his Ph.D. thesis (*A steady thermohaline convection model*, Univ. Miami, 1979) and unpublished manuscripts.

References

Baines, W.D., Turner, J.S., 1969. Turbulent buoyant convection from a source in a confined region. Journal of Fluid Mechanics 37, 51–80.

Beardsley, R.C., Festa, J.F., 1972. A numerical model of convection driven by a surface stress and non-uniform heating. Journal of Physical Oceanography 2, 444–455.

Bryan, F., 1987. Parameter sensitivity of primitive equation ocean general circulation models. Journal of Physical Oceanography 17, 970–985.

Bryan, K., Cox, M., 1967. A numerical investigation of oceanic general circulation. Tellus 19, 54–80.

Choboter, P.F., Swaters, G.E., 2000. On the baroclinic instability of axisymmetric rotating gravity currents with bottom slope. Journal of Fluid Mechanics 408, 149–177.

Defant, A., 1961. Physical oceanography, vol. I. MacMillan, New York, USA.

Döscher, R., Redler, R., 1997. The relative importance of northern overflow and subpolar deep convection for the North Atlantic thermohaline circulation. Journal of Physical Oceanography 27, 1894–1902.

England, M.H., 1995. The age of water and ventilation timescales in a global ocean model. Journal of Physical Oceanography 25, 2756–2777.

Etling, D., Gelhardt, F., Schrader, U., Brennecke, F., Kühn, G., Chabert d'Hieres, G., Didelle, H., 2000. Experiments with density currents on a sloping bottom in a rotating fluid. Dynamics of Atmospheres and Oceans 31, 139–164.

Fahrbach, E., Harms, S., Rohardt, G., Schröder, M., Woodgate, R.A., 2001. Flow of bottom water in the northwestern Weddell Sea. Journal of Geophysical Research 106, 2761–2778.

Foldvik, A., Gammelsrød, T., Østerhus, S., Fahrbach, E., Rohardt, G., Schröder, M., Nicholls, K.W., Padman, L., Woodgate, R.A., 2004. Ice shelf water and bottom water formation in the southern Weddell Sea. Journal of Geophysical Research 109, C02015. doi:10.1029/2003JC002008.

Ganachaud, A., 2003. Large-scale mass transports, water mass formation, and diffusivities estimated from World Ocean Circulation Experiment (WOCE) hydrographic data. Journal of Geophysical Research 108, 3213. doi:10.1029/2002JC001565.

Ganachaud, A., Wunsch, C., 2000. Improved estimates of global ocean circulation, heat transport and mixing from hydrographic data. Nature 408, 453–457.

Gill, A.E., 1982. Atmosphere-ocean Dynamics. Academic Press, London, England.

Gregg, M.C., 1989. Scaling turbulent dissipation in the thermocline. Journal of Geophysical Research 94, 9686–9698.

Griffiths, R.W., 1986. Gravity currents in rotating systems. Annual Reviews in Fluid Mechanics 18, 59–89.

Griffiths, R.W., Hopfinger, E.J., 1984. The structure of mesoscale turbulence and horizontal spreading at ocean fronts. Deep-Sea Research 31, 245–269.

Griffiths, R.W., Linden, P.F., 1982. Laboratory experiments on fronts. Part 1. Density-driven boundary currents. Geophysical and Astrophysical Fluid Dynamics 19, 159–187.

Griffiths, R.W., Killworth, P.D., Stern, M.E., 1982. Ageostrophic instability of ocean currents. Journal of Fluid Mechanics 117, 343–377.

Hignett, P., Ibbetson, A., Killworth, P.D., 1981. On rotating thermal convection driven by non-uniform heating from below. Journal of Fluid Mechanics 109, 161–187.

Hodnett, P., McNamara, R., 2003. On the spatial variation of the vertical thermal diffusion coefficient in a simple ocean model. Mathematical Proceedings of the Royal Irish Academy 103A, 217–230.

Houghton, J.T., Meira Filho, L.G., Callander, B.A., Harris, N., Kattenberg, A., Maskell, K., 1996. Climate Change 1995: The Science of Climate Change. Cambridge University Press, Cambridge, England.

Huang, R.X., 1999. Mixing and energetics of the oceanic thermohaline circulation. Journal of Physical Oceanography 29, 727–746.

Jeffreys, H.T., 1925. On fluid motions produced by differences of temperature and humidity. Quarterly Journal of the Royal Meteorological Society 51, 347–356.

Jiang, L., Garwood Jr., W., 1996. Three-dimensional simulations of overflows on continental slopes. Journal of Physical Oceanography 26, 1224–1233.

Killworth, P.D., 2001. On the rate of descent of overflows. Journal of Geophysical Research 106, 22267–22275.

Killworth, P.D., Manins, P.C., 1980. A model of confined thermal convection driven by non-uniform heating from below. Journal of Fluid Mechanics 98, 587–607.

Killworth, P.D., Turner, J.S., 1982. Plumes with time-varying buoyancy in a confined region. Geophysical and Astrophysical Fluid Dynamics 20, 265–291.

Kunze, E., Sanford, T.B., 1996. Abyssal mixing: Where is it not? Journal of Physical Oceanography 26, 2286–2296.

Ledwell, J.R., Watson, A.J., Law, C.S., 1993. Evidence for slow mixing across the pycnocline from an open-ocean tracer release experiment. Nature 364, 701–703.

Ledwell, J.R., Montgomery, E.T., Polzin, K.L., St. Laurent, L.C., Schmitt, R.W., Toole, J.M., 2000. Evidence for enhanced mixing over rough topography in the abyssal ocean. Nature 403, 179–182.

Legg, S., Hallberg, R.W., Girton, J.B., in press. Comparison of entrainment in overflows simulated by z-coordinate, isopycnal and nonhydrostatic models. Ocean Modelling, doi:10.1016/j.ocemod.2004.11.006.

Lueck, R.G., Mudge, T.D., 1997. Topographically induced mixing around a shallow seamount. Science 276, 1831–1833.

MacCready, P., Johns, W.E., Rooth, C.G., Fratantoni, D.M., Watlington, R.A., 1999. Overflow into the deep Caribbean: effects of plume variability. Journal of Geophysical Research 104, 25913–25935.

Manins, P.C., 1973. A filling box model of the deep circulation of the Red Sea. Mémoires Société Royale des Sciences de Liége 6, 153–166.

Manins, P.C., 1979. Turbulent buoyant convection from a source in a confined region. Journal of Fluid Mechanics 91, 765–781.

Marotzke, J., Scott, J., 1999. Convective mixing and the thermohaline circulation. Journal of Physical Oceanography 29, 2962–2970.

Matear, R.J., Wong, C.S., 1997. Estimation of vertical mixing in the upper ocean at Station P from chlorofluorocarbons. Journal of Marine Research 55, 507–521.

Mensch, M., Bayer, R., Bullister, J.L., Schlosser, P., Weiss, R.F., 1996. The distribution of tritium and CFCs in the Weddell Sea during the mid-1980s. Progress in Oceanography 38, 377–415.

Mori, A., Niino, H., 2002. Time evolution of nonlinear horizontal convection: its flow regimes and self-similar solutions. Journal of the Atmospheric Sciences 59, 1841–1856.

Mullarney, J.C., 2004. Thermal and Thermohaline Convection Models for the Meridional Overturning Circulation of the Oceans. Ph.D. thesis, The Australian National University.

Mullarney, J.C., Griffiths, R.W., Hughes, G.O., 2004. Convection driven by differential heating at a horizontal boundary. Journal of Fluid Mechanics 516, 181–209.

Munk, W.H., 1966. Abyssal recipes. Deep-Sea Research 13, 707–730.

Munk, W.H., Wunsch, C., 1998. Abyssal recipes II: energetics of tidal and wind mixing. Deep-Sea Research I 45, 1977–2010.

Orsi, A.H., Johnson, G.C., Bullister, J.L., 1999. Circulation, mixing, and production of Antarctic Bottom Water. Progress in Oceanography 43, 55–109.

Orsi, A.H., Smethie Jr., W.M., Bullister, J.L., 2002. On the total input of Antarctic waters to the deep ocean: a preliminary estimate from chlorofluorocarbon measurements. Journal of Geophysical Research 107. doi:10.1029/2001JC000976.

Paparella, F., Young, W.R., 2002. Horizontal convection is non-turbulent. Journal of Fluid Mechanics 466, 205–214.

Park, Y., Bryan, K., 2000. Comparison of thermally driven circulation from a depth-coordinate model and an isopycnal model. Part I: Scaling law sensitivity to vertical diffusion. Journal of Physical Oceanography 30, 590–605.

Park, Y., Bryan, K., 2001. Comparison of thermally driven circulation from a depth-coordinate model and an isopycnal model. Part II: The difference and structure of the circulations. Journal of Physical Oceanography 31, 2612–2624.

Park, Y.G., Whitehead, J.A., 1999. Rotating convection driven by differential bottom heating. Journal of Physical Oceanography 29, 1208–1220.

Peixoto, J.P., Oort, A.H., 1992. Physics of climate. American Institute of Physics, New York.

Pierce, D.W., Rhines, P.B., 1996. Convective building of a pycnocline: laboratory experiments. Journal of Physical Oceanography 26, 176–190.

Polzin, K.L., Toole, J.M., Ledwell, J.R., Schmitt, R.W., 1997. Spatial variability of turbulent mixing in the abyssal ocean. Science 276, 93–96.

Price, J.F., Baringer, M.O., 1994. Outflows and deep water production by marginal seas. Progress in Oceanography 33, 161–200.

Price, J.F., Sanford, T., Mauritzen, C., 2003. Faroe Bank Channel over-flow. EOS, Transactions, American Geophysical Union 84(52), Ocean Science Meeting Supplement, Abstract OS41H-04.

Rahmstorf, S., 1996. On the freshwater forcing and transport of the Atlantic thermohaline circulation. Climate Dynamics 12, 799–811.

Rahmstorf, S., 2003. The current climate. Nature 421, 699.

Rossby, H.T., 1965. On thermal convection driven by non-uniform heating from below: an experimental study. Deep-Sea Research 12, 9–16.

Rossby, H.T., 1998. Numerical experiments with a fluid non-uniformly heated from below. Tellus 50, 242–257.

Rudnick, D.L., Boyd, T.J., Brainard, R.E., Carter, G.S., Egbert, G.D., Gregg, M.C., Holloway, P.E., Klymak, J.M., Kunze, E., Lee, C.M., Levine, M.D., Luther, D.S., Martin, J.P., Merrifield, M.A., Moum, J.N., Nash, J.D., Pinkel, R., Rainville, L., Sanford, T.B., 2003. From tides to mixing along the Hawaiian ridge. Science 301, 355–357.

Sandström, J.W., 1908. Dynamische versuche mit meerwasser. Annalen der Hydrographic und Maritimen Meteorologie 36, 6–23.

Scott, J.R., Marotzke, J., 2003. The location of diapycnal mixing and the meridional overturning. Journal of Physical Oceanography 33, 118–135.

Send, U., Marshall, J., 1995. Integral effects of deep convection. Journal of Physical Oceanography 25, 855–872.

Sloyan, B.M., Rintoul, S.R., 2001. The Southern Ocean limb of the global deep overturning circulation. Journal of Physical Oceanography 31, 143–173.

Spall, M.A., Pickart, R.S., 2001. Where does dense water sink? A subpolar gyre example. Journal of Physical Oceanography 31, 810–826.

Speer, K., Tziperman, E., 1990. Convection from a source in an ocean basin. Deep-Sea Research 37, 431–446.

Stommel, H., 1962. On the smallness of sinking regions in the ocean. Proceedings of the National Academy of Sciences, Washington 48, 766–772.

Stommel, H., Arons, A.B., 1960. On the abyssal circulation of the world ocean—II. An idealized model of the circulation pattern and amplitude in oceanic basins. Deep-Sea Research 6, 217–233.

Suginohara, N., Aoki, S., 1991. Buoyancy-driven circulation as horizontal convection on beta-plane. Journal of Marine Research 49, 295–320.

Sutherland, B.R., Nault, J., Yewchuck, K., Swaters, G.E., 2004. Rotating currents on a slope. Part 1. Stability. Journal of Fluid Mechanics 508, 241–264.

Swaters, G.E., 1991. On the baroclinic instability of cold-core coupled density fronts on a sloping continental shelf. Journal of Fluid Mechanics 224, 361–382.

Swaters, G.E., 1998. Numerical simulation of the baroclinic dynamics of density-driven coupled fronts and eddies on a sloping bottom. Journal of Geophysical Research 103, 2945–2962.

Thorpe, R.B., Wood, R.A., Mitchell, J.F.B., 2004. Sensitivity of the modelled thermohaline circulation to the parameterisation of mixing across the Greenland–Scotland ridge. Ocean Modelling 7, 259–268.

Tsujino, H., Suginohara, N., 1999. Thermohaline circulation enhanced by wind forcing. Journal of Physical Oceanography 29, 1506–1516.

Tsujino, H., Hasumi, H., Suginohara, N., 2000. Deep Pacific circulation controlled by vertical diffusivity at the lower thermocline depths. Journal of Physical Oceanography 30, 2853–2865.

Turner, J.S., 1973. Buoyancy Effects in Fluids. Cambridge University Press, Cambridge, England.

Turner, J.S., 1986. Turbulent entrainment: the development of the entrainment assumption, and its application in geophysical flows. Journal of Fluid Mechanics 173, 431–471.

Visbeck, M., Marshall, J., Jones, H., 1996. Dynamics of isolated convection regions in the ocean. Journal of Physical Oceanography 26, 1721–1734.

Wang, W., Huang, R.X., in press. An experimental study on thermal convection driven by horizontal differential heating. Journal of Fluid Mechanics.

Webb, D., Suginohara, N., 2001. Oceanography—vertical mixing in the ocean. Nature 409, 37.

Weppernig, R., Schlosser, P., Khatiwala, S., Fairbanks, R.G., 1996. Isotope data from Ice Station Weddell: implications for deep water formation in the Weddell Sea. Journal of Geophysical Research 101, 25723–25739.

Whitehead, J.A., Pedlosky, J., 2000. Circulation and boundary layers in differentially heated rotating stratified fluid. Dynamics of Atmospheres and Oceans 31, 1–21.

Winton, M., 1995. Why is the deep sinking narrow? Journal of Physical Oceanography 25, 997–1005.

Wong, A.B.D., Griffiths, R.W., 2001. Stratification and convection produced by multiple plumes. Dynamics of Atmospheres and Oceans 30, 101–123.

Wright, D.G., Stocker, T.F., 1991. A zonally averaged ocean model for the thermohaline circulation. Part I: Model development and flow dynamics. Journal of Physical Oceanography 21, 1713–1724.

Wunsch, C., 2000. Moon, tides & climate. Nature 405, 743–744.

Wunsch, C., Ferrari, R., 2004. Vertical mixing, energy, and the general circulation of the oceans. Annual Reviews in Fluid Mechanics 36, 281–314.